Astronomy & Astrophysics manuscript no. 4596
February 5, 2008

Evolutionary state of magnetic chemically peculiar stars ⋆,⋆⋆

O. Kochukhov[1] and S. Bagnulo[2]

[1] Department of Astronomy and Space Physics, Uppsala University, SE-751 20, Uppsala, Sweden
[2] European Southern Observatory, Casilla 19001, Santiago 19, Chile

Received 28 November 2005 / Accepted 16 January 2006

ABSTRACT

Context. The photospheres of about 5–10 % of the upper main sequence stars exhibit remarkable chemical anomalies. Many of these chemically peculiar (CP) stars have a global magnetic field, the origin of which is still a matter of debate.
Aims. We present a comprehensive statistical investigation of the evolution of magnetic CP stars, aimed at providing constraints to the theories that deal with the origin of the magnetic field in these stars.
Methods. We have collected from the literature data for 150 magnetic CP stars with accurate Hipparcos parallaxes. We have retrieved from the ESO archive 142 FORS1 observations of circularly polarized spectra for 100 stars. From these spectra we have measured the mean longitudinal magnetic field, and discovered 48 new magnetic CP stars (five of which belonging to the rare class of rapidly oscillating Ap stars). We have determined effective temperature and luminosity, then mass and position in the H-R diagram for a final sample of 194 magnetic CP stars.
Results. We found that magnetic stars with $M > 3\,M_{\odot}$ are homogeneously distributed along the main sequence. Instead, there are statistical indications that lower mass stars (especially those with $M \leq 2\,M_{\odot}$) tend to concentrate in the centre of the main sequence band. We show that this inhomogeneous age distribution cannot be attributed to the effects of random errors and small number statistics. Our data suggest also that the surface magnetic flux of CP stars increases with stellar age and mass, and correlates with the rotation period. For stars with $M > 3\,M_{\odot}$, rotation periods decrease with age in a way consistent with the conservation of the angular momentum, while for less massive magnetic CP stars an angular momentum loss cannot be ruled out.
Conclusions. The mechanism that originates and sustains the magnetic field in the upper main sequence stars may be different in CP stars of different mass.

Key words. stars: chemically peculiar – stars: evolution – stars: fundamental parameters – stars: magnetic fields

1. Introduction

Observations suggest that magnetic fields are ubiquitous in late-type stars, and that a correlation exists between magnetic activity and stellar rotation. The magnetic field of late-type stars is typically localised in spots, and evolves on relatively short time scales. Although not yet fully understood, a *dynamo* mechanism is commonly invoked to explain the presence of a magnetic field in these kinds of stars.

Early-type stars show a completely different magnetic phenomenology. Magnetic fields appear organised on a large-scale at the stellar surface, and do not change within a time scale shorter than several decades. Instead, a periodic field variability is observed, which is commonly interpreted in terms of the so-called *Oblique Rotator Model*: the magnetic field geometry is not symmetric about the rotation axis, and the observer sees a magnetic configuration that changes as the star rotates. The field strength (typically a few hundreds up to a few tens of thousands of Gauss) does not seem correlated to the star's rotational velocity. Only a minority (about 5 %) of early-type stars is magnetic. Practically all known magnetic stars of the upper main sequence are classified between late F- and early B-type, and belong to the category of the so-called *chemically peculiar* (CP) stars, i.e., stars that exhibit distinctive peculiarities in the element abundance of their atmospheres. Most CP stars (hence most magnetic stars) show also abnormally slow rotation.

The origin of the magnetic fields in CP stars is a matter of debate (Moss 2004). The dynamo hypothesis can hardly explain the observed high field strengths and the lack of a correlation with rotation. A more promising approach is offered by the *fossil field* theory (Cowling 1945; Moss 1989; Braithwaite & Spruit 2004), according to which the observed fields in the upper main sequence magnetic stars are the remnants of fields present during earlier stages of stellar evolution. The fact that no correlation is observed with stellar rotation, and the fact that only a small percentage of the upper main sequence stars are magnetic, are naturally explained in terms of variations

Send offprint requests to: O. Kochukhov, e-mail: oleg@astro.uu.se
⋆ Tables 1 and 2 are only available in electronic form at http://www.edpsciences.org
⋆⋆ Based on observations made with ESO Telescopes at the Paranal Observatory under programs ID 71.D-0308, 72.D-0377, and 73.D-0464, retrieved through the ESO archive.

in the amount of magnetic flux trapped during star formation. However, it not yet clear (observationally nor theoretically) if and how these fields evolve during the main sequence phase.

To provide constraints to the theory of the origin of the magnetic field, it is important to study the *evolutionary state* of magnetic CP stars. This has been done by several authors, and with conflicting conclusions. Based on a small sample of about 30 magnetic stars, Hubrig et al. (2000) suggested that magnetic fields appear at the surface of CP stars with $M \lesssim 3\,M_{\odot}$ only after they have spent considerable fraction of their life on the main sequence. Most low mass stars studied by Hubrig et al. (2000) were drawn from the group of very slowly rotating magnetic stars with detectable Zeeman splitting in their spectra (Mathys et al. 1997). This selection procedure results in a statistic sample small in size, that may also be intrinsically biased toward older stars (should the star's angular momentum be lost or/and the surface magnetic field increase during the main sequence evolutionary phase). Both Gomez et al. (1998) and Pöhnl et al. (2005) investigated much larger samples of CP stars, but instead of selecting objects for which magnetic field was detected, they utilised chemical peculiarity as a proxy of magnetism. They have found that CP stars with chemical anomalies similar to those observed in magnetic CP stars occupy all the regions of the main sequence.

In an attempt to clarify this puzzling situation, we have carried out a new study of the evolution of magnetic stars of the upper main sequence that is based on a very large sample of observed magnetic CP stars, collected through a thoroughfull investigation of the literature and of the ESO archive. Our study includes all known objects for which precise parallaxes were measured by the Hipparcos mission, and for which the presence of magnetic field at the surface could be asserted via direct field detections. We have also investigated whether there are observational evidences for angular momentum losses occurring during the star's evolution in the main sequence.

This paper is organised as follows. Section 2 describes the observations collected from the literature, and presents new magnetic measurements obtained from the analysis of data collected with FORS1 at the ESO VLT. In Sect. 3 we determine the temperature and luminosity of the selected stellar sample, and in Sect. 4 we derive the position of the selected stars in the H-R diagram. Results and statistical analysis are presented in Sect. 5 and discussed in Sect. 6.

2. The stellar sample

2.1. Known magnetic stars

The main part of our sample of magnetic CP stars has been drawn from various literature sources. The catalogues by Romanyuk (2000) and Bychkov et al. (2003) have provided the core of the sample of the early-type stars with definite magnetic field detections. Since the present study focuses on the classical magnetic Ap/Bp stars, we have selected objects with the SrCrEu, Si, and/or He chemical peculiarities for which reliable detection of magnetic field has been obtained with one of the two direct methods: spectropolarimetric or photopolarimetric measurement of the disk-averaged line of sight (longitudinal) magnetic field (Mathys 1991; Borra & Landstreet 1980) and the mean field modulus diagnostic using resolved Zeeman split spectral line profiles (Mathys et al. 1997).

The list of stars compiled from the two catalogues was supplemented by a number of recently discovered magnetic stars. In particular, the studies by Aurière et al. (2004), El'kin et al. (2003), Johnson (2004), Hubrig et al. (2003, 2005), Ryabchikova et al. (2004, 2005), Shorlin et al. (2002), and Stütz et al. (2003) have provided objects satisfying our selection criteria. We refer the reader to the original papers for the description of the respective observations and their analysis. Putting aside details of these studies of individual magnetic CP stars, it is worth noting that all investigations mentioned above relied on the classical direct methods of the magnetic field detection (spectropolarimetry and/or measurement of the resolved Zeeman split lines) and that only objects with reliable ($> 3\sigma$ in the case of longitudinal field measurements) magnetic field detections were included in our sample.

According to the current understanding of the incidence of magnetism in early-type stars, the non-magnetic chemically peculiar stars, including objects with the HgMn and Am peculiarity types, do not host global magnetic fields similar to those found in the classical magnetic CP stars. Although claims of the detection of magnetic field in HgMn or Am stars have occasionally been made (e.g., Mathys & Lanz 1990; Hubrig & Castelli 2001), these studies typically employed an indirect diagnostic of magnetic field based on the analysis of magnetic broadening and intensification of spectral lines. Furthermore, none of the alleged detections of the complex fields in non-magnetic CP stars was confirmed by a subsequent, independent observation or supported by direct spectropolarimetric magnetic field diagnostic technique (Shorlin et al. 2002; Wade et al. 2003). Given this absence of the solid evidence for the presence of significant surface fields in HgMn and Am stars, all such objects were eliminated from our list of magnetic stars. We emphasise that in nearly all cases when non-zero longitudinal field determinations are reported for HgMn or Am stars in the catalogues compiled by Romanyuk (2000) and Bychkov et al. (2003), the original measurements date back to the early low-precision spectropolarimetric observations by Babcock (1958).

The magnetic stellar sample compiled in the present study was cross-matched with the Hipparcos parallax data (Perryman et al. 1997). Parallaxes with an accuracy better than 20% (which is the same threshold as employed by Hubrig et al. 2000) could be retrieved for 150 magnetic CP stars. Magnetic field in the majority of these stars was detected using polarimetric observations. Consequently, unlike the 33 magnetic stars studied by Hubrig et al. (2000), our sample does not suffer from the possible bias of over-representing the slowly rotating and strongly magnetic old stars for which resolved Zeeman split lines are observable.

2.2. Magnetic stars observed with FORS1 at VLT

FORS1 (FOcal Reducer/low dispersion Spectrograph) of the ESO VLT is a multi-mode instrument equipped with polarisation analysing optics including super-achromatic half-wave

and quarter-wave phase retarder plates, and a Wollaston prism. In the last few years, FORS1 has been extensively used in polarimetric mode to measure magnetic fields in various kinds of stars, for instance in white dwarfs (e.g., Aznar Cuadrado et al. 2004), in hot subdwarfs (O'Toole et al. 2005), in the central stars of planetary nebulae (Jordan et al. 2005). In particular, several observing programs have been dedicated to the magnetic field surveys of Ap stars, and many data are now available in the ESO archive. For this work we have retrieved 142 observations of circular polarised spectra for a total of 100 Ap stars. All targets have been observed using grism 600 B and a 0.4″ slit-width, which gives a spectral resolution of about 2000, covering the spectral range 3550–5850 Å. A typical observing block consists of four frames obtained with the $\lambda/4$ retarder waveplate oriented at +45° and four frames obtained with the retarder waveplate at −45°. Data have been reduced using standard IRAF routines in order to get wavelength calibrated spectra from the ordinary and extra-ordinary beams taken with the $\lambda/4$ retarder waveplate oriented at +45° and −45°. From these spectra we have obtained Stokes I and V profiles using Eq. (4.1) of the FORS1+2 User Manual (VLT-MAN-ESO-13100-1543), but with the sign changed. We have then considered the Stokes I and V profiles of the Balmer lines from Hβ down to the Balmer jump, and then we have obtained the longitudinal field $\langle B_z \rangle$ using a least-square technique based on the formula

$$\frac{V}{I} = -g_{\rm eff}\, C_{\rm z}\, \lambda^2\, \frac{1}{I}\, \frac{{\rm d}I}{{\rm d}\lambda}\, \langle B_{\rm z} \rangle\ , \qquad (1)$$

where $g_{\rm eff}$ is the effective Landé factor (= 1 for the hydrogen Balmer lines, see Casini & Landi Degl'Innocenti 1994), λ is the wavelength expressed in Å, $\langle B_z \rangle$ is the longitudinal field expressed in Gauss, and

$$C_{\rm z} = \frac{e}{4\pi m_{\rm e} c^2} \quad (\simeq 4.67 \times 10^{-13}\ {\rm \AA}^{-1}\ {\rm G}^{-1}),$$

where e is the electron charge, $m_{\rm e}$ the electron mass, c the speed of light. Equation (1) is valid under the weak-field approximation, which, for the hydrogen Balmer lines formed in a typical atmosphere of an A-type star, holds for field strength up to ~ 20 kG. More details on the data reduction technique, and the way $\langle B_z \rangle$ is calculated, are given in Bagnulo et al. (2002) and Bagnulo et al. (2005).

The new $\langle B_z \rangle$ measurements are reported in Table 1 (available in electronic form only). Magnetic field was detected at $> 3\sigma$ level in 53 stars. Only five of them were previously known to be magnetic, whereas the other four lack accurate parallax data in the Hipparcos catalogue. Thus, analysis of the archival FORS1 spectra has contributed with 44 magnetic stars, increasing the total sample investigated in the present paper to 194 objects.

We note that definite detection of the longitudinal field in five members (HD 19918, HD 42659, HD 60435, HD 84041, HD 86181) of the rare class of rapidly oscillating Ap (roAp) stars is reported here for the first time, thereby significantly increasing the number of roAp stars with known magnetic field properties.

3. Determination of effective temperatures and luminosities

3.1. Photometric effective temperature

Stellar effective temperatures were determined using calibration of the Geneva photometric system (Golay 1972). Observed photometric parameters were extracted from the catalogue of Rufener (1989) and supplemented by the data available through the online photometric database at Geneva Observatory[1]. We determined $T_{\rm eff}$ of CP stars following the procedure suggested by Hauck & North (1993) and revised by Hauck & Künzli (1996). For hot stars calibration in the theoretical grids published by Künzli et al. (1997) was used in combination with the linear $T_{\rm eff}$ correction to account for anomalous flux distribution of magnetic CP stars (Hauck & Künzli 1996). For cool Ap stars we employed calibration of the $(B2-G)_0$ color index proposed by Hauck & North (1993).

For a few CP stars lacking photometric measurements in the Geneva system we determined $T_{\rm eff}$ using Strömgren *uvbyβ* photometric data (Hauck & Mermilliod 1998) and calibration by Moon & Dworetsky (1985).

Effective temperature of the extreme cool magnetic peculiar star HD 101065 (Przybylski's star) cannot be determined using any usual calibrations available either for normal or CP stars. Instead, a $T_{\rm eff} = 6450$ K was adopted for this object based on the results of recent detailed spectroscopic studies (Cowley et al. 2000; Kochukhov et al. 2002). The spectroscopic $T_{\rm eff} = 7750$ K (Kochukhov et al. 2002) was also used for HD 216018, which lacks a complete set of Strömgren or Geneva photometry.

For a subsample of stars with both Strömgren and Geneva photometry available, uncertainty of effective temperature can be estimated from the discrepancy of $T_{\rm eff}$ values given by independent calibrations in the two different photometric systems. Based on this assessment we adopted $\sigma(T_{\rm eff}) = 200$ K for stars with $T_{\rm eff} \le 8500$ K, $\sigma(T_{\rm eff}) = 300$ K for $8500 < T_{\rm eff} \le 10500$ K, $\sigma(T_{\rm eff}) = 400$ K for $10500 < T_{\rm eff} \le 16000$ K, and $\sigma(T_{\rm eff}) = 500$ K for stars hotter than $T_{\rm eff} = 16000$ K. These error estimates are very similar to the $T_{\rm eff}$ uncertainty assumed by Hubrig et al. (2000, see their tables 1 and 2), although no explicit discussion of the adopted $T_{\rm eff}$ error bars can be found in the latter paper.

3.2. Correction for the interstellar extinction and reddening

The interstellar extinction and reddening have to be taken into account for stars located farther away than 60 pc. We considered four different procedures to obtain color excess $E(B-V)$ for individual stars in our sample: from the intrinsic $[U-B]$ color and reddening-free Geneva X and Y parameters of hotter stars (Cramer 1982), from the interstellar extinction maps of Lucke (1978) and Schlegel et al. (1998), and using the model of Hakkila et al. (1997). The $E(B-V)$ parameters obtained from these sources were averaged after rejection of occasional outliers. Based on the scatter of the color excess values de-

[1] http://obswww.unige.ch/gcpd/ph13.html

rived using different methods, we found a typical uncertainty of $E(B-V)$ to be 0.005 mag for $E(B-V) \leq 0.05$ and 0.010 mag for $E(B-V) > 0.05$. For several strongly reddened objects a higher $E(B-V)$ error bar had to be adopted, reflecting large standard deviation of highly discrepant reddening estimates.

Photometric parameters in the Geneva and Strömgren system were dereddened with the help of relations based on the interstellar extinction laws given by Fitzpatrick (1999). Interstellar extinction in the V-band was calculated using $R \equiv A_V/E(B-V) = 3.1$.

3.3. Hipparcos luminosity

Absolute magnitudes and luminosities of the program stars were determined on the basis of data from the Hipparcos catalogue (Perryman et al. 1997) and the V-magnitude information extracted from the SIMBAD database. Distribution of the Hipparcos parallaxes and their relative errors is illustrated in Fig. 1. Most of the studied stars are located within 250 pc from the Sun, but only a few are closer than 60 pc. The average parallax uncertainty for the magnetic stars in our sample is 11%. Roughly half of the stars have parallax determined with an accuracy better than that.

From the comparison of magnitudes given in different literature sources, we estimated uncertainty of m_V related to the measurement errors and intrinsic stellar variability to be approximately 0.02 mag.

For a number of magnetic stars known to be members of spectroscopic or unresolved visual binaries we applied positive duplicity correction to m_V. Generally, this correction can be estimated from the luminosity ratios available from literature for the majority of well-studied SB2 and visual binaries. On the other hand, CP stars belonging to SB1 systems usually lack precise luminosity ratio estimates. For these objects we adopted $\Delta m_V = 0.16$ which corresponds to the magnitude difference of 2.0 between components.

The absolute magnitude in the V-band was determined using the standard relation:

$$M_V = m_V + 5 + 5\log\pi - A_V, \tag{2}$$

where trigonometric parallax π is measured in arcseconds and interstellar extinction was determined as outlined above. The error estimate for the absolute magnitude took into account uncertainties in m_V, π, and A_V:

$$\sigma(M_V) = \sqrt{\sigma^2(m_V) + \left(\frac{5\sigma(\pi)}{\pi \ln 10}\right)^2 + \sigma^2(A_V)}. \tag{3}$$

Calculating the stellar luminosity,

$$\log\frac{L}{L_\odot} = -\frac{M_V + BC - M_{\rm bol}(\odot)}{2.5}, \tag{4}$$

we adopted the solar bolometric magnitude $M_{\rm bol}(\odot) = +4.75$ (Bessell 2000) and used the standard bolometric correction BC taken from Flower (1996). Since in the latter paper BC is tabulated as a function of $T_{\rm eff}$, uncertainty of effective temperature contributes to the total error of luminosity that can be estimated according to the following expression:

$$\sigma\left(\log\frac{L}{L_\odot}\right) = 0.4\sqrt{\sigma^2(M_V) + \left(\frac{{\rm d}BC}{{\rm d}T_{\rm eff}}\right)^2 \sigma^2(T_{\rm eff})}. \tag{5}$$

Taking into account all contributions to the M_V and $L/L_\odot$ error budgets, we find a typical uncertainty of 20–25% for both parameters.

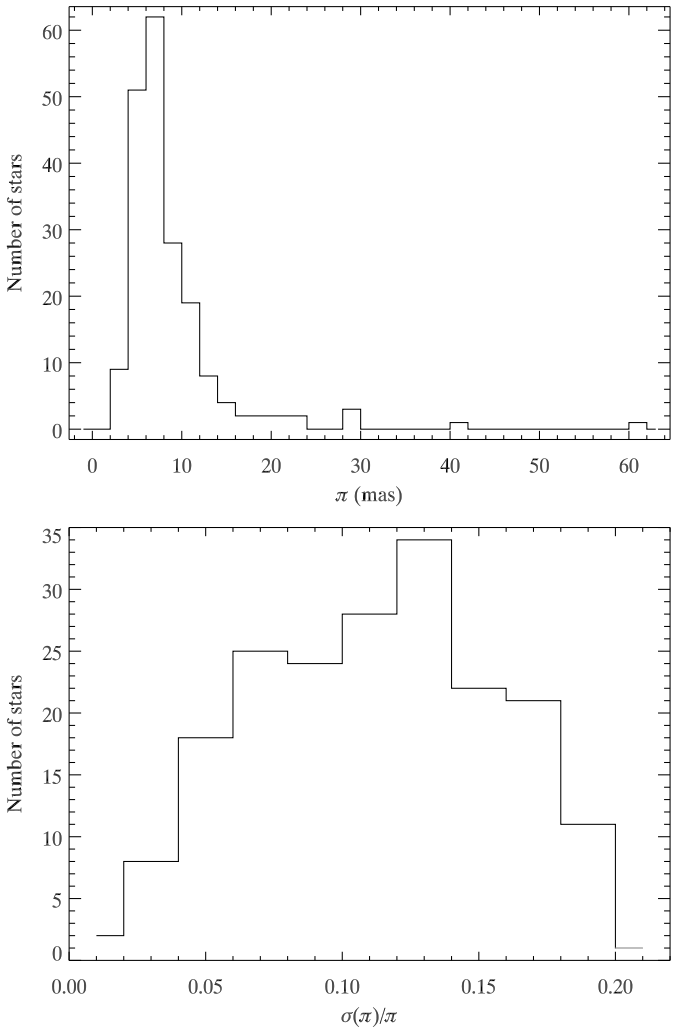

Fig. 1. Distribution of the Hipparcos parallaxes (*top*) and their relative errors (*bottom*) for the sample of magnetic CP stars.

Anomalous flux distribution of peculiar stars is characterized by the enhanced ultraviolet absorption which induces backwarming in the visible (Leckrone 1973). This makes CP stars sub-luminous for their visual colours, and bolometric correction has to be modified accordingly (North 1981; Lanz 1984). In the present paper we use BC tabulated as a function of $T_{\rm eff}$ for normal stars (Flower 1996). However, we account for peculiar nature of CP stars in derivation of their $T_{\rm eff}$ (Sect. 3.1). With this procedure the average change in BC due to anomalous stellar flux distribution is taken into account implicitly. Remaining modifications of BC depend on individual properties of magnetic stars and are difficult to estimate without detailed model atmosphere analysis. Nevertheless, this BC un-

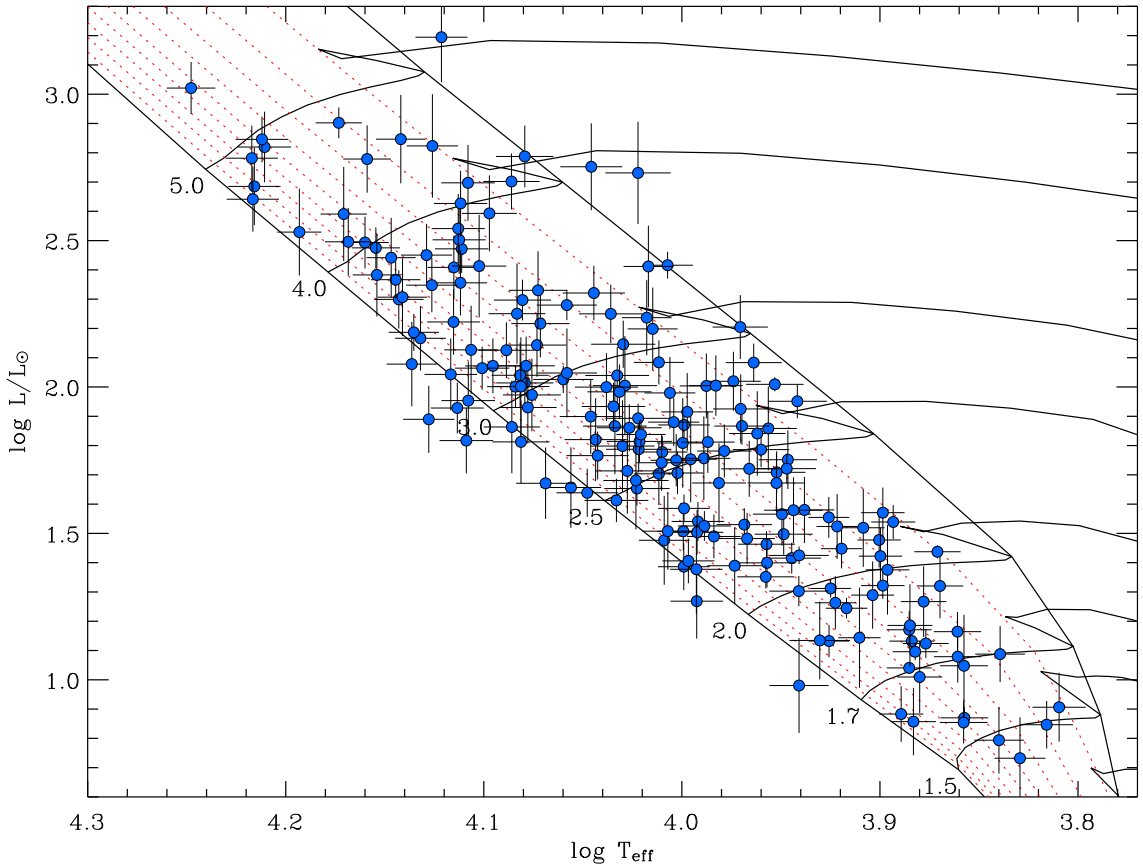

Fig. 2. Position of magnetic chemically peculiar stars on the Hertzsprung-Russell diagram. The solid lines show theoretical evolutionary tracks, the ZAMS and the envelope of lowest $T_{\rm eff}$ achieved during the main sequence evolutionary stage (Schaller et al. 1992; Schaerer et al. 1993). Dotted curves correspond to the lines of equal fractional age τ measured in units of the main sequence stellar lifetime. These curves are plotted with a step of 0.1 between the ZAMS ($\tau = 0$) and the end of the core hydrogen burning phase ($\tau = 1$).

certainty is likely to be much smaller compared to the average error of $M_{\rm bol}$ (0.24 mag) for the stars in our sample.

No Lutz-Kelker (LK, Lutz & Kelker 1973) correction was applied to the absolute magnitudes of magnetic stars in our sample. The original LK correction, which is always negative and hence systematically increases luminosity estimated from parallax, has been a source of confusion and extensive debate in literature. In a recent publication Smith (2003) summarised this discussion and concluded that the LK correction is meaningful only when applied to the stellar samples, but should not be used in studies of individual stars. As pointed out by Stępień (2004), large (from −0.1 mag up to −0.5 mag) negative LK corrections adopted by Hubrig et al. (2000) displaced the stars in their sample significantly upwards from the zero age main sequence (ZAMS), possibly resulting in apparent lack of young low mass magnetic stars. A similar problem may have affected results of Pöhnl et al. (2005) who, contrary to the recommendations of Smith (2003) and Stępień (2004), have also attempted to use the LK procedure to correct individual stellar magnitudes.

4. Mass and age determination

Theoretical evolutionary tracks of the upper main sequence stars are available for different metal abundance of the stellar envelope (see Schaller et al. 1992 and Schaerer et al. 1993). Large deviations of the chemical composition of CP stars from the normal solar abundance table are believed to be limited to the surface layers. These superficial chemical anomalies are produced by the process of selective radiative diffusion in the presence of magnetic field, stellar wind, and possibly weak turbulent mixing. These complex hydrodynamical effects are poorly understood and hence it is not possible to estimate the average interior metal content of individual CP stars based on the observed surface abundance pattern. In this situation a fixed, usually solar, metallicity has to be assumed to make comparison of the observed and predicted stellar parameters possible (e.g., Hubrig et al. 2000; Pöhnl et al. 2005). Here we have adopted metallicity $Z = 0.018$ and obtained theoretical stellar evolutionary tracks by interpolating within the grids of Schaerer et al. (1993) and Schaller et al. (1992), who published calculations for $Z = 0.008$ and $Z = 0.020$, respectively. The plausible effect of the dispersion in Z can be estimated from the scatter in the surface abundances determined for normal B stars and nearby young F and G stars. Using the summary of

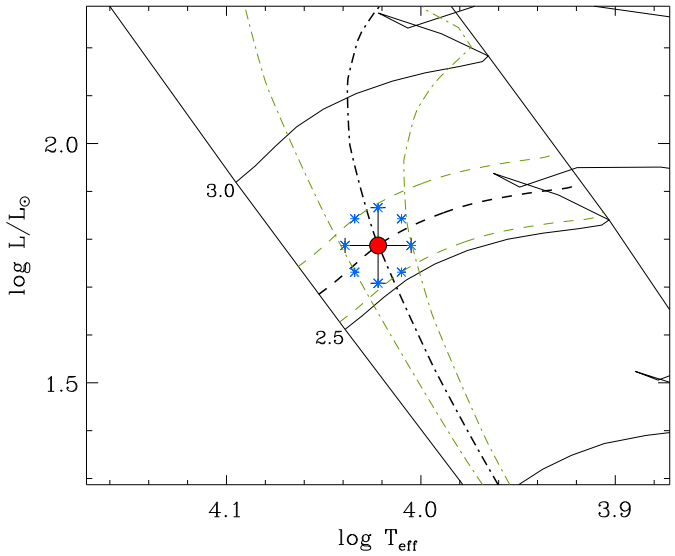

Fig. 3. Illustration of the error analysis applied to derive asymmetric confidence intervals for the stellar mass and age. The solid lines show theoretical evolutionary tracks (Schaller et al. 1992; Schaerer et al. 1993). The point and error bars indicate our estimate of the temperature and luminosity of the magnetic CP star HD 56350. Thick dashed and dash-dotted lines correspond to interpolated evolutionary tracks and isochrones, respectively. Interpolation procedure is repeated for 8 locations along the error ellipse in the log $T_{\rm eff}$–log $L/L_\odot$ plane, as shown by asterisks. Thin dashed and dash-dotted curves show tracks and isochrones for minimum and maximum mass and age. This analysis yields a stellar mass $M/M_\odot = 2.610^{+0.090}_{-0.088}$ and age log $t = 8.40^{+0.11}_{-0.21}$ yr.

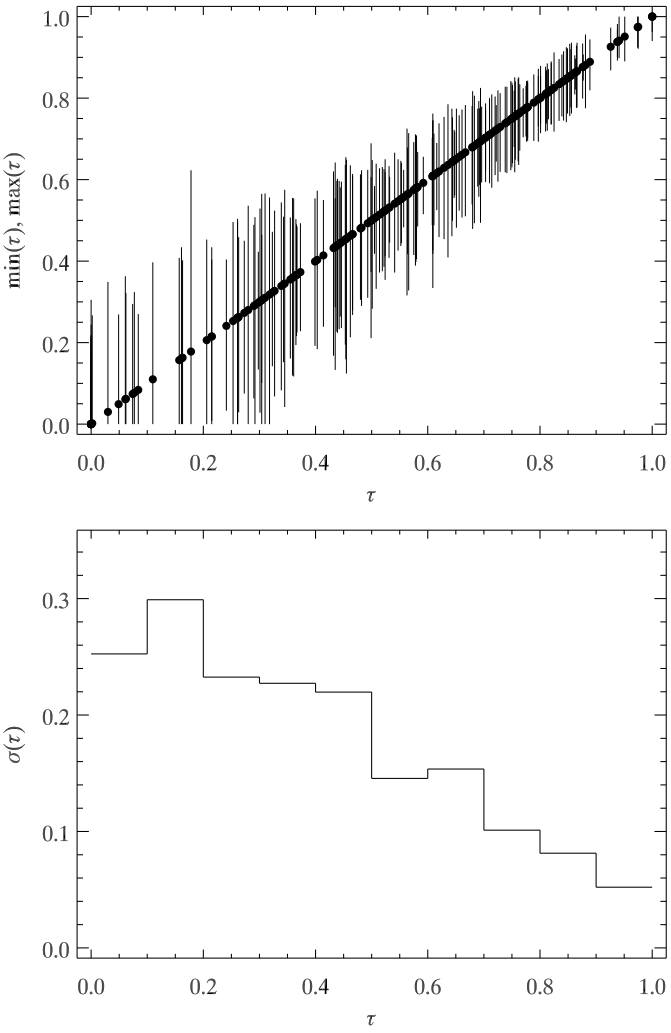

Fig. 4. Distribution of 1σ confidence intervals of the fractional ages (*top*) and respective mean error bar (*bottom*) as a function of the relative stellar age for the studied sample of magnetic stars.

the Fe and light element abundances given by Sofia & Meyer (2001), we obtain star-to-star Z variation of ≈ 0.002. The resulting effect on the age and mass determination of CP stars is smaller than other error sources.

Figure 2 illustrates distribution of magnetic CP stars in the theoretical H-R diagram. Each star is shown with a point, whereas respective error bars give uncertainty of $T_{\rm eff}$ and luminosity. The ZAMS and the envelope of the lowest $T_{\rm eff}$ achieved during the core hydrogen burning phase are also shown. Given a set of theoretical isochrones, the problem of the stellar mass determination reduces to interpolation within the evolutionary tracks tabulated for different masses. To avoid degeneracy, all stars were assumed to lie within the main sequence zone where $T_{\rm eff}$ decreases monotonously. For a few objects located below the ZAMS or above the lowest $T_{\rm eff}$ line, parameters were calculated for the closest main sequence point.

Subsequent determination of the stellar age is complicated by the uneven evolution of stars in the log $T_{\rm eff}$–log $L/L_\odot$ plane. Young stars located close to the ZAMS change their temperature and luminosity very slowly. The pace of evolution increases rapidly as the star ages and shifts towards the terminal age main sequence. Therefore, the same uncertainty of $T_{\rm eff}$ and L translates into dramatically different age errors, depending on whether the star is young or evolved. Although this effect is well-known, to our knowledge, no attempt has ever been made to take it properly into account in the statistical studies of the evolutionary state of CP stars. In the present paper we developed a non-linear error propagation procedure to obtain realistic errors of the absolute and relative ages. For each star in our sample we determined mass and age for the point corresponding to the adopted stellar log $T_{\rm eff}$ and log $L/L_\odot$ and then repeated this procedure for 8 positions along the error ellipse defined by the individual uncertainty of temperature and luminosity. Resulting minimum and maximum ages yield realistic asymmetric range of evolutionary stages compatible with a given pair of $T_{\rm eff}$ and L and their respective 1σ error limits. Application of this non-linear error propagation procedure to the magnetic CP star HD 56350 is illustrated in Fig. 3.

The summary of the age confidence limits is given in Fig. 4. Here and elsewhere in the paper we quantify the relative stellar age, τ, by the fraction of the stellar life spent on the main sequence. The ZAMS line corresponds to $\tau = 0$, whereas the star at the end of the core hydrogen burning phase has $\tau = 1$. As it follows from Fig. 4, the relative age of individual young CP stars cannot be determined with an accuracy better than ≈ 20 %.

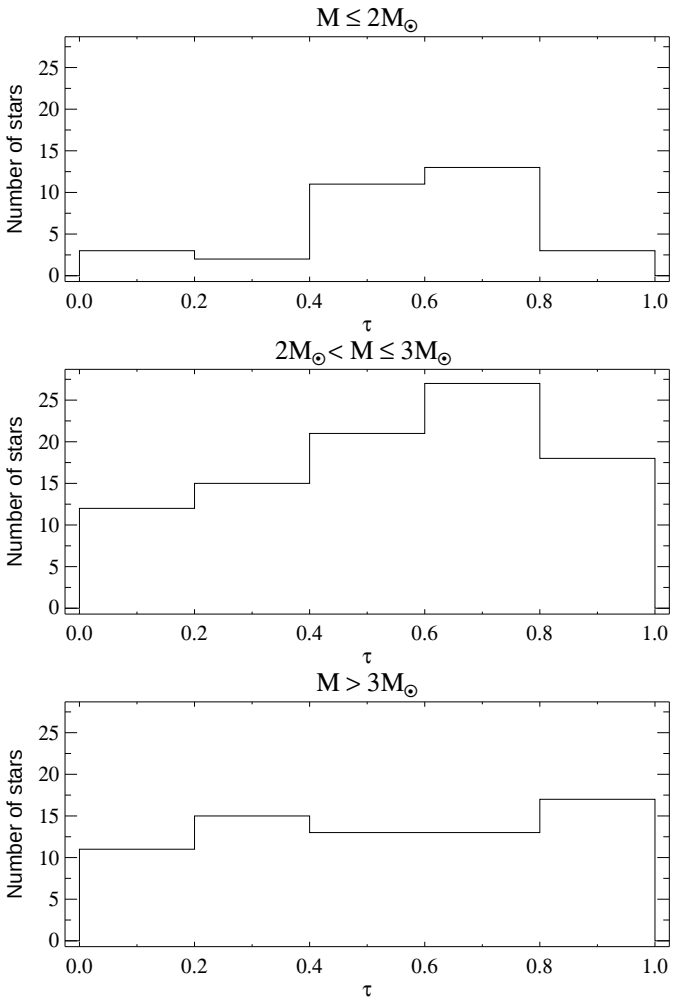

Fig. 5. Distribution of the relative ages for magnetic CP stars of different mass.

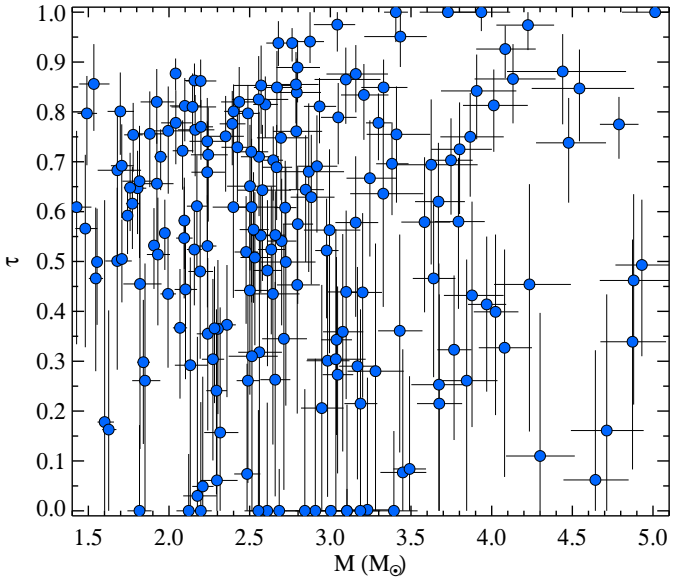

Fig. 6. Distribution of magnetic CP stars in the $\tau - M$ plane.

Only for the oldest stars in our sample the H-R diagram fitting yields ages precise at the 5–7 % level.

The final set of the stellar fundamental parameters and corresponding 1σ (68 %) confidence intervals is reported in Table 2 (available in electronic form only). For each star we list its identification in the HD and Hipparcos catalogues, distance, absolute magnitude, effective temperature, luminosity, mass, absolute and relative ages. Using the data in Table 2, is also straightforward to estimate the stellar radius

$$\log(R/R_\odot) = 0.5\log(L/L_\odot) - 2\log(T_{\rm eff}/T_{\rm eff\odot}) \quad (6)$$

and the surface gravitational acceleration

$$\log(g/g_\odot) = \log(M/M_\odot) + 4\log(T_{\rm eff}/T_{\rm eff\odot}) - \log(L/L_\odot). \quad (7)$$

5. Results

5.1. Distribution of stars in the H-R diagram

We have grouped all magnetic stars in our sample into three different mass bins: stars with $M \le 2M_\odot$, stars with $2M_\odot < M \le 3M_\odot$, and stars with $M > 3M_\odot$. Figure 5 shows the distribution of the relative ages for the stars belonging to these three groups. An alternative overview of the age distribution of the magnetic stars of various masses is given in Fig. 6. We found that 26 % of stars with mass $> 3\,M_\odot$ have spent less than 30 % of their life in the main sequence. This percentage is 18 % for stars with mass between $2\,M_\odot$ and $3\,M_\odot$, and only 16 % for stars with $M \le 2\,M_\odot$. It appears thus that higher mass stars ($M > 3M_\odot$) are homogeneously distributed in fractional age. In the group of stars of intermediate mass, younger stars seem less numerous than older stars. Among stars with $M \le 2\,M_\odot$ the shortage of young objects is even more pronounced.

The statistical validity of these results must be carefully investigated, since *a priori* one could argue that a small sample of objects randomly selected from a homogeneous group may well be characterized by special features that in fact are not representative of the entire sample. In other words, one could suspect that the apparent shortage of young magnetic stars with $M \le 3\,M_\odot$ is just the result of a statistical fluctuation. It should also be noted that young stars are those for which age determination is less accurate. In order to clarify this situation, we have performed numerical simulations to calculate what is the probability that, repeating the same study, one obtains a number of stars with $\tau < 0.3$ equal or smaller than what we have found. This estimates the false alarm probability, i.e. the chance that the observed uneven distribution of stellar ages can be attributed to a statistical fluctuation.

First of all, we have given an analytical representation to the error bars of the fractional age, by using a linear fit to the values given in Table 2. Namely, we have estimated the lower and upper error bars as

$$\Delta\tau_- = 0.33 - 0.29\,\tau \ \text{ and } \ \Delta\tau_+ = 0.27 - 0.26\,\tau, \quad (8)$$

respectively. Then we have considered a sample of N objects. To each of them, we have associated a random number p_i from 0.0 to 1.0, representing the fractional age. Each p_i number has been transformed to a $p_i' = p_i + \delta(p_i)$ value, where the "errors" $\delta(p_i)$ were deduced from a Gaussian distribution with standard deviation $\Delta\tau_-$ (for $\delta(p) < 0$) or $\Delta\tau_+$ (for $\delta(p) > 0$), using again

a random number generator. All $p'_i < 0$ have been then set to 0, and all $p'_i > 1$ have been changed to 1. We have then counted the number J_k of p'_i values included within the interval $[0.0, 0.3]$. We have repeated the same exercise M times, and finally counted the number L of times in which J_k was equal or smaller than a certain number Q. The ratio $P_1(N, Q) = L/M$ gives the probability that, in a sample of N stars homogeneously distributed in fractional age, we find no more than Q stars in the interval $[0.0, 0.3]$.

In our observational sample of $N = 32$ magnetic stars with $M \leq 2M_\odot$, we have found only 5 stars with $\tau \leq 0.3$. Therefore we have performed the statistical test described above using $N = 32$ and $Q = 5$, and calculated $P_1(32, 5) = 6.5\,\%$. We have also found that in the sample of 93 magnetic stars with $2M_\odot < M \leq 3\,M_\odot$, 17 have $\tau \leq 0.3$. For this case, the statistical test gives $P_1(93, 17) = 1.3\,\%$. Finally, we have found that 18 over 69 magnetic stars with $M > 3\,M_\odot$ have $\tau \leq 0.3$, and we have calculated $P_1(69, 18) = 36\,\%$.

It is also of interest to test a complementary hypothesis that magnetic stars belong to a homogeneous population of objects with a relative age of at least $\tau = 0.3$, and all young stars in our sample appear entirely due to observational errors. In order to investigate this possibility, we have repeated the simulations choosing the fractional age randomly in the interval $[0.3, 1.0]$ and counting trials in which the number stars with $\tau < 0.3$ has reached the observed value. The resulting probability, $P_2(N, Q)$, turns out to be considerable for stars with $M \leq 2M_\odot$ ($P_2 = 23\,\%$) but is negligible ($P_2 \lesssim 1\,\%$) for more massive stars.

Another conspicuous feature of the stellar age distributions presented in Figs. 5 and 6 is the relatively small number of $M \leq 3\,M_\odot$ stars at the end of their main sequence life. Stellar evolution is fast in this region of the H-R diagram. Consequently, the relative age is determined with good precision (see Fig. 4). Applying the same statistical approach as outlined above (for stars in the $[0.0, 1.0]$ age interval) we could, however, verify that the lack of stars with $\tau \geq 0.8$ is not particularly significant by itself: the corresponding false alarm probability, $P_3(N, Q)$ is 7 % and 40 % for the two groups of low mass stars ($M \leq 2\,M_\odot$ and $2\,M_\odot < M \leq 3\,M_\odot$, respectively), and $P_3 = 81\,\%$ for stars with $M > 3\,M_\odot$.

We have further extended the statistical analysis to test the possibility that the *overall* shape of the observed distribution of stellar ages can be attributed to random errors and effects of small number statistics. This was achieved by computing the composite probability that, given the number of objects observed in each mass range, the fraction of stars in the relative age interval $[0.0, 0.4]$ (the sum of the first two bins in the histograms of Fig. 5) and, simultaneously, of those in the $[0.8, 1.0]$ interval (the last bin in Fig. 5) does not exceed the observed values. We have found that the observed strong concentration of stars in the middle of the H-R diagram is seldom realised in a random sample of low mass stars drawn from a homogeneous age distribution. Denoting the corresponding probability with P_4, we have obtained $P_4 = 0.004\,\%$ and $P_4 = 0.6\,\%$ for stars with $M \leq 2M_\odot$ and $2M_\odot < M \leq 3M_\odot$, respectively. At the same time, for stars with $M > 3\,M_\odot$ we have determined $P_4 = 39\,\%$.

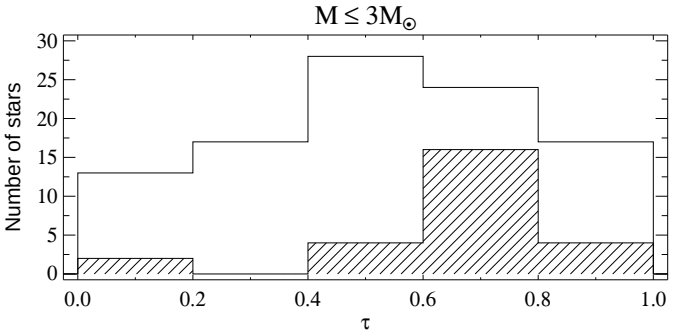

Fig. 7. Distribution of the relative ages for magnetic CP stars in the $M \leq 3\,M_\odot$ mass group. The hatched histogram shows the age distribution for stars with the resolved Zeeman split lines, whereas the other histogram corresponds to stars without detectable Zeeman splitting.

The conclusion of this series of tests is that it is very unlikely that the picture we have found is due to random errors in the determination of the stellar fundamental parameters. Unless the methods employed to measure stellar temperature and luminosity are affected by some large systematic errors, and assuming that the evolutionary models are correct, the following scenario emerges from our study. Magnetic stars with $M \leq 3M_\odot$ are concentrated in the centre of the H-R diagram, and, in this mass range, older stars are more numerous than younger magnetic stars. In particular, the age distribution of stars with $M \leq 2M_\odot$ might even be explained by a parent population entirely older that $\tau \approx 0.3$, scattered by random errors, whereas a similar interpretation is unlikely for stars with $2\,M_\odot < M \leq 3\,M_\odot$. In the latter mass range, young magnetic stars are found more rarely than expected from a distribution that is homogeneous in age, but they do exist. There are also strong indications of a lack of lower mass stars in the final stages of the main sequence evolution. Finally, magnetic CP stars with $M > 3\,M_\odot$ are homogeneously distributed in age.

Detection of the Zeeman resolved split lines was reported for 26 stars included in our sample. They all have masses below $3\,M_\odot$ and constitute only 13 % of the whole sample, which should be compared with nearly 70 % of such objects in the sample analysed by Hubrig et al. (2000). In Fig. 7 we compare the age distributions of magnetic stars with and without magnetically split lines. It is clear that stars with the Zeeman resolved lines are more evolved and may not be representative of the parent population of magnetic CP stars.

5.2. Magnetic field

Homogeneous determination of the H-R diagram position for the large sample of magnetic CP stars allows us to investigate evolutionary changes of the surface magnetic field strength and to probe its possible dependence on the fundamental stellar parameters. We have considered the average quadratic longitudinal field (Borra et al. 1983) defined with the equation

$$\langle \overline{B_z} \rangle = \left(\frac{1}{N} \sum_{i=1}^{N} \langle B_z \rangle_i^2 \right)^{1/2} \qquad (9)$$

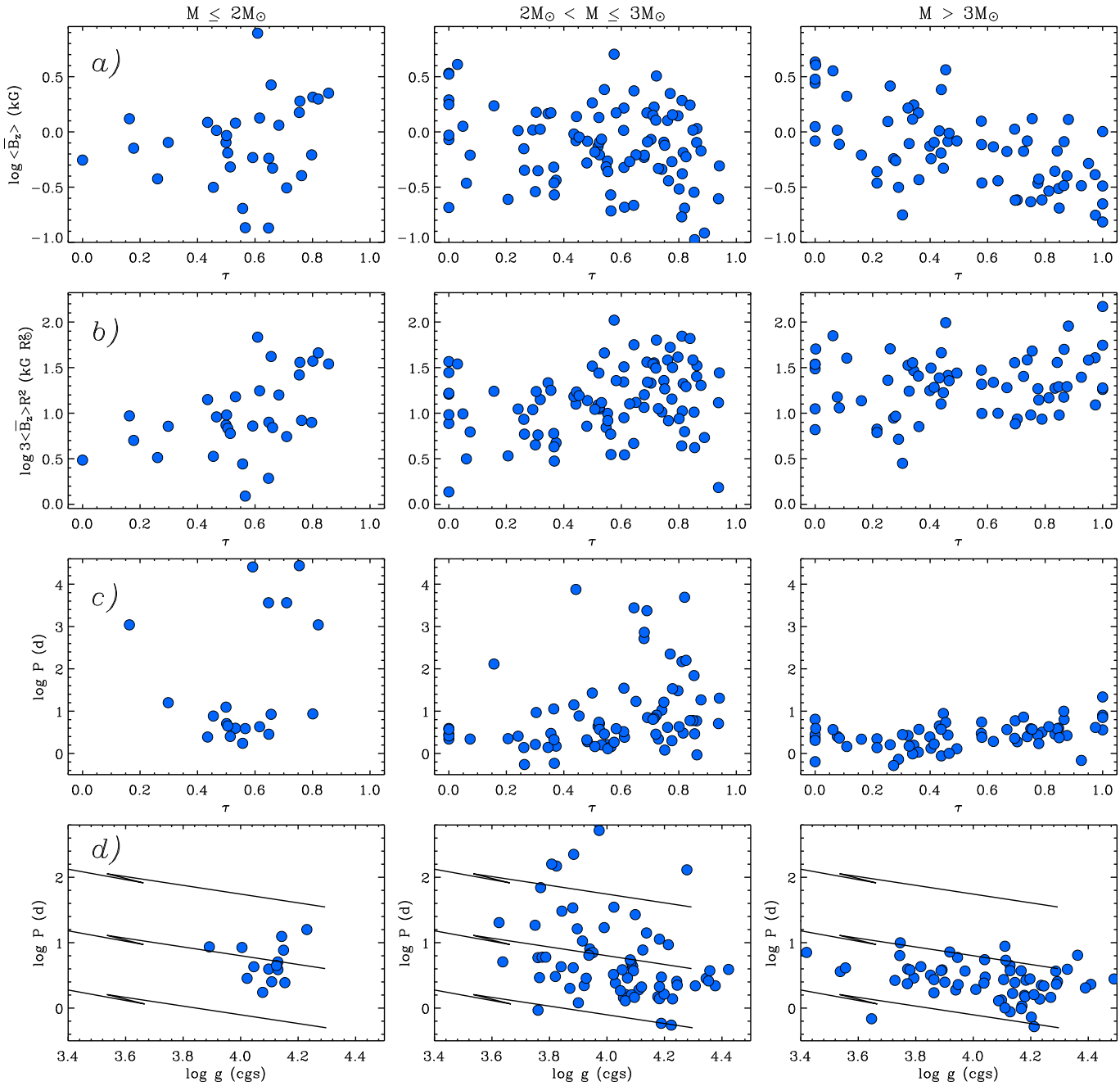

Fig. 8. The average longitudinal magnetic field (**a)**), magnetic flux (**b)**), and rotation period (**c)**) as a function of the relative age for magnetic CP stars with $M \leq 2\,M_\odot$ (*left column*), $2\,M_\odot < M \leq 3\,M_\odot$ (*middle column*), and $M > 3\,M_\odot$ (*right column*). The bottom panels (**d)**) show rotation period as a function of surface gravity. The solid lines represent evolution of the rotation period (for initial periods of 0.5, 4, and 35 days) expected for the situation when the angular momentum is conserved.

as magnetic field strength estimator. When available, the $\langle\overline{B_z}\rangle$ estimates were taken from the catalogue by Bychkov et al. (2003), otherwise we have computed $\langle\overline{B_z}\rangle$ from the individual longitudinal field measurements of the newly detected magnetic CP stars. For a few stars magnetic field was only observed using Zeeman resolved lines in the intensity spectra. In this case we have used approximate relation $\langle\overline{B_z}\rangle \approx \langle B_s\rangle/3$ to bring these field modulus magnetic measurements on the same scale with the average longitudinal field estimates. In addition to the observed magnetic field strength, we have computed the quantity $3\langle\overline{B_z}\rangle R^2$, which is proportional to the unsigned magnetic flux and hence provides a possibility to distinguish intrinsic evolutionary changes of the magnetic field intensity from the secular variation of the surface field strength caused by increase in the stellar radii.

The average longitudinal field and magnetic flux as a function of the relative stellar age τ are presented in Fig. 8a and b, where different panels correspond to the three mass bins defined above. Dependence of the magnetic quantities on the stellar rotation period and mass are shown in Fig. 9 and 10,

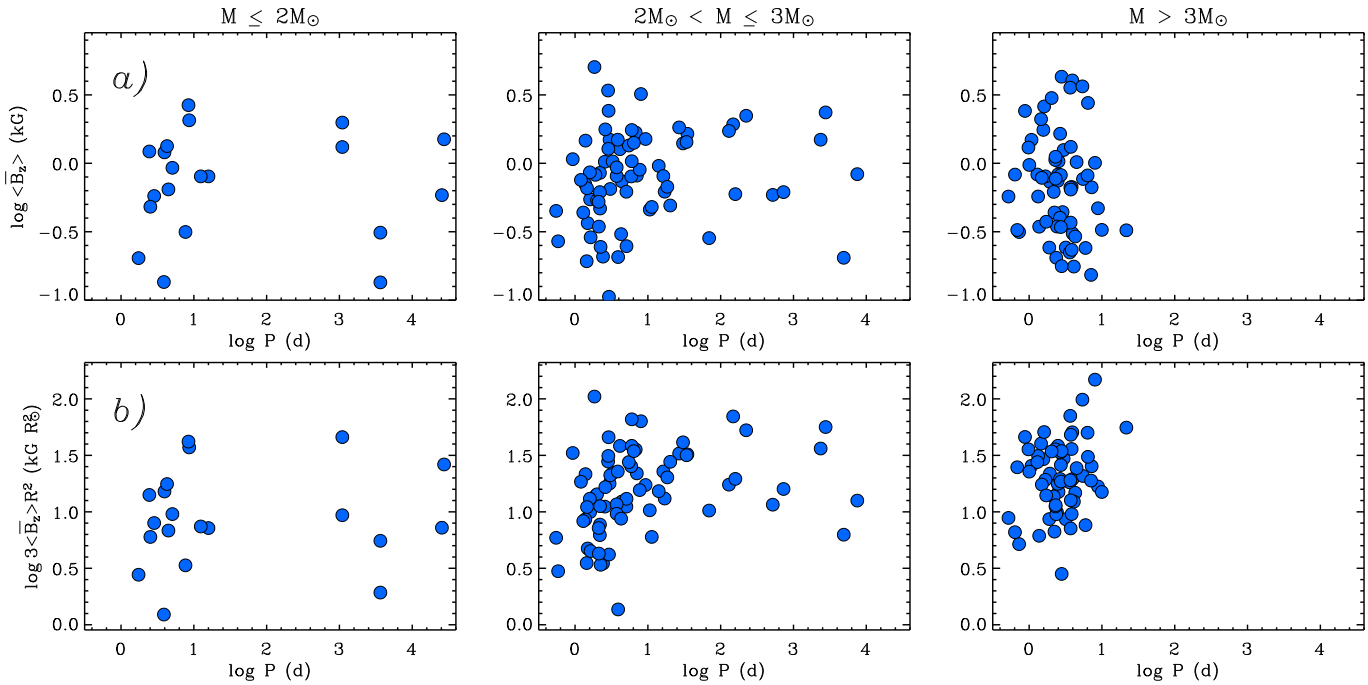

Fig. 9. The average longitudinal magnetic field (**a)**) and magnetic flux (**b)**) as a function of rotation period.

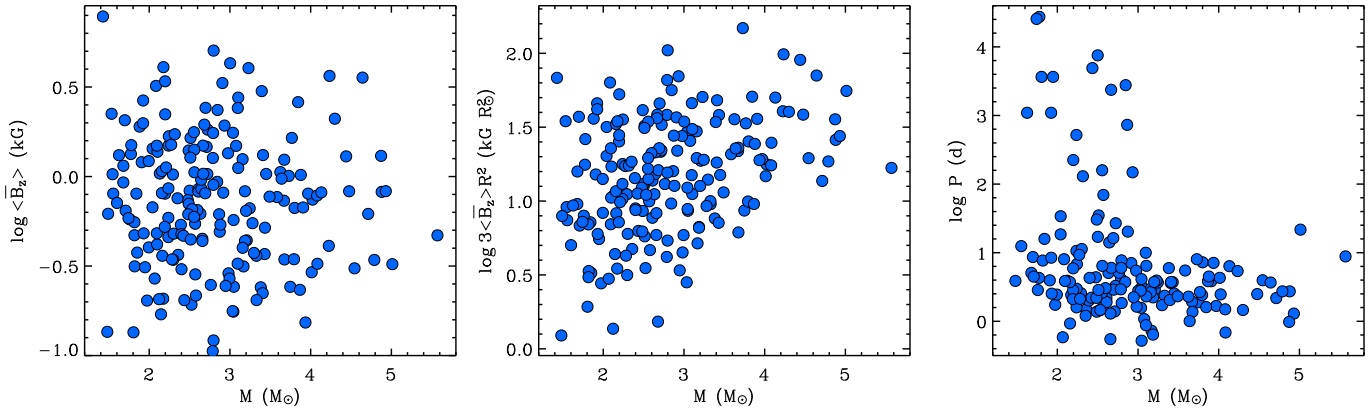

Fig. 10. The average longitudinal magnetic field (*left panel*), magnetic flux (*middle panel*), and rotation period (*right panel*) as a function of stellar mass.

respectively. The non-parametric Spearman's rank correlation coefficient r (Press et al. 1992) and the associated significance D were used to quantify dependencies of the magnetic quantities on the stellar parameters.

The plot of $\langle\overline{B_z}\rangle$ against elapsed fraction of the main sequence life reveals a significant anticorrelation ($r = -0.29$, $D > 99.9\,\%$) for the whole stellar sample and for the individual groups of stars, except for the low mass ($M \leq 2M_\odot$) objects. However, when the strong evolutionary increase of the stellar radii is accounted for, significant positive correlation ($r = 0.24$, $D > 99.9\,\%$) between the magnetic flux and τ becomes evident. This trend is significant in the group of $M \leq 3M_\odot$ stars and marginal for stars with $M > 3M_\odot$. On the basis of this analysis we can draw the conclusion that the magnetic flux in the surface layers of low mass ($M \leq 3M_\odot$) CP stars increases with time. On average, the magnetic flux grows by almost a factor of 4 between $\tau = 0$ and $\tau = 1$. This effect is far less prominent (flux increase of about 40 % at the $D = 75\,\%$ significance level) in the magnetic stars with $M > 3M_\odot$.

No trend of the average longitudinal field with the stellar mass is present in our data (Fig. 10). At the same time, unambiguous correlation ($r = 0.35$, $D > 99.9\,\%$) emerges if we consider the magnetic flux as a function of mass. We have determined the average magnetic fluxes 15.2 ± 0.5, 19.3 ± 0.2, and 27.2 ± 0.3 (in the 4πkG$R_\odot^2$ units) for the $M \leq 2M_\odot$, $2M_\odot < M \leq 3M_\odot$, and $M > 3M_\odot$ mass ranges, respectively. Thus, our investigation leads to the conclusion that massive stars are intrinsically more magnetic compared to low mass CP objects.

Information on the rotation periods of the magnetic stars in our sample was obtained from the catalogue of Catalano & Renson (1998) and was further supplemented with the period measurements reported in several recent studies (Paunzen & Maitzen 1998; Koen & Eyer 2002; Ryabchikova et al. 2005).

Estimates of rotation periods could be found for 80 % of stars from our sample. A relation between the average longitudinal field and stellar rotation (see Fig. 9) reveals a marginal (D = 86 %) correlation, which is the strongest (D = 98 %) in the group of stars with $2M_\odot < M \leq 3M_\odot$. This trend is reinforced if the magnetic flux is considered instead of the average longitudinal field. In this case, we have found $r = 0.19$, D = 98 % for the whole sample and a definite correlation ($D > 99.9$ %) for stars in the intermediate mass range. These results indicate that the surface field is more intense in slowly rotating magnetic CP stars.

5.3. Stellar rotation

We have investigated evolutionary changes of the stellar rotation periods and studied a relation between rotation and fundamental stellar parameters. Rotation period as a function of the relative age, surface gravity, and stellar mass is presented in Fig. 8c, Fig. 8d, and Fig. 10, respectively. We have found a clear evidence that older stars have longer rotation periods. This trend is significant ($r = 0.37$, $D > 99.9$ %) for the whole sample and for the two groups of stars with $M > 2M_\odot$ ($D > 99.8$ %). A marginal correlation (D = 80 %) is also found for the low mass objects ($M \leq 2M_\odot$).

A prominent dependence of rotation period on mass is revealed by our statistical analysis (see Fig. 10). Rotation periods of the most massive ($M > 3M_\odot$) magnetic CP stars show a fairly sharp cutoff at $P_{\rm rot} \approx 10$ days. In contrast, there are many instances of much slower rotation among less massive ($M \leq 3M_\odot$) CP stars.

Possible changes of the total angular momentum and secular evolution of the stellar moment of inertia can both contribute to the observed variation of rotation periods. In order to isolate a signature of the angular momentum evolution, we have followed North (1998) and studied rotation period as a function of surface gravity. In Fig. 8d the observed relation is compared with the changes of rotation period predicted for rigidly rotating stars that conserve the total angular momentum during their life at the main sequence. These theoretical curves, adopted from North (1998), are virtually mass independent and are plotted in Fig. 8d for initial periods of 0.5, 4, and 35 days. From this comparison we have found that the observed period-age dependence of stars with $M > 3M_\odot$ is fully accounted for by the changes of the moment of inertia. Thus, we see no indication of significant changes in the angular momentum of the most massive magnetic CP stars. At the same time, the group of stars in the $2M_\odot < M \leq 3M_\odot$ mass range shows an abnormally steep slope in their $\log P_{\rm rot}$–$\log g$ diagram, suggesting that these stars may have experienced some loss of the angular momentum during the main sequence evolutionary stage. If we subtract theoretically expected period trend from our data, a marginal residual anticorrelation ($r = -0.13$, D = 71 %) of rotation period with respect to $\log g$ is still present. The large scatter of data points precludes us from quantifying the angular momentum evolution history of the low mass magnetic CP stars in more detail.

6. Discussion and conclusions

We have carried out a detailed statistical investigation of the evolutionary state of the upper main sequence magnetic CP stars. The sample of 194 objects has included all CP stars whose magnetic status could be confirmed with a direct detection of the surface magnetic field and for which precise parallax is available in the Hipparcos catalogue. The literature data on the magnetic observations of CP stars were complemented with the analysis of the archival spectropolarimetric data acquired with the FORS1 instrument at ESO VLT. This allowed us to detect magnetic field in 53 A and B-type CP stars, of which only five were previously known to be magnetic. Using the medium-band (Geneva or Strömgren) photometry of the program stars, we have determined $T_{\rm eff}$ and then have placed stars on the H-R diagram. We were able to obtain stellar masses, radii, and ages from the comparison of the observed luminosity and temperature with the predictions of the theoretical evolutionary tracks. Our investigation has included a comprehensive non-linear error analysis, that has permitted us to quantify uncertainty of the derived stellar properties for each period of the main sequence life. Numerical simulations were applied to assess the properties of the resulting age distributions of the magnetic CP stars of different masses. We have also employed correlation analysis to study dependence of the surface magnetic field, magnetic flux, and rotation period on the stellar mass and to probe possible evolutionary changes of the stellar rotation and magnetic field.

The key results of our study can be summarised as follows.

1. The most massive magnetic CP stars ($M > 3M_\odot$) are distributed homogeneously in the main sequence band. On the other hand, stars with $M \leq 3M_\odot$ show the tendency to cluster in the middle of the main sequence. The relative shortage of young and very old stars is especially pronounced in the group of low mass ($M \leq 2M_\odot$) stars. This uneven age distribution cannot be attributed to the effect of random errors in determination of the stellar parameters.

2. We have found 22 young ($\tau \leq 0.3$) magnetic stars among the objects with $M \leq 3M_\odot$, thereby rejecting the proposal by Hubrig et al. (2000) that all observably magnetic low mass CP stars have completed significant fraction of their main sequence evolution. At the same time, our data for the least massive ($M \leq 2M_\odot$) stars is not inconsistent with a population of stars older than $\tau = 0.3$.

3. The average surface field observed in magnetic CP stars decreases with time. However, for stars with $M \leq 3M_\odot$ this decrease is slower than the field weakening computed under the assumption of the magnetic flux conservation. Consequently, we suggest that the surface magnetic flux of the low mass CP stars increases with time.

4. Comparison of the average magnetic fluxes of the CP stars from different mass ranges shows that massive CP stars are substantially more magnetic. At the same time, we found a correlation between magnetic field and rotation period for

the intermediate mass stars.

5. Rotation period of magnetic stars increases with time, but for stars with $M > 3M_\odot$ the stellar structure changes influencing the stellar moment of inertia can fully account for the observed period increase. On the other hand, our results do not rule out the possibility that angular momentum losses occur during the main sequence evolution of stars with $2\,M_\odot < M \leq 3\,M_\odot$.

The conspicuous inhomogeneous age distribution of the low mass magnetic CP stars which has emerged from our statistical analysis requires careful verification and interpretation. Our results raise the question whether the anomalous H-R diagram distribution is the property of stars with significant surface magnetic field or it is intrinsic to the whole group of the SrCrEu and less massive Si-type stars. No significant anomalies in the evolutionary state of these subclasses of CP stars were reported by Gomez et al. (1998). However, the adopted upper threshold of the relative parallax uncertainty and the methods used in the Gomez et al. study differ substantially from the analysis procedure employed in the present investigation. Methodologically more similar analysis by Pöhnl et al. (2005) included only 15 stars with $M \leq 2\,M_\odot$, and most of these objects were found in the centre of the main sequence band, very similar to our results.

An indirect hint that the SrCrEu and Si chemical peculiarity is closely related to the presence of magnetic field at the stellar surface comes from the survey of bright Ap stars carried out by Aurière et al. (2004). Using sensitive spectropolarimetric field diagnostic methods, these authors were able to detect magnetic field in essentially every peculiar star they have observed and have established a possible lower threshold of ≈ 250 G for the strength of the dipolar field component. In the light of these findings and taking results of our study into account, an investigation of the evolutionary status of *all* SrCrEu and Si stars with $M \leq 3\,M_\odot$ would be of great importance and could benefit from the upcoming revision of the Hipparcos data reduction (van Leeuwen & Fantino 2005).

For many decades the problem of the evolution of global magnetic field in A and B stars was approached in the framework of the analysis of the Ohmic decay of the poloidal fossil field, assumed to exist in stellar interior (Cowling 1945; Moss 1984; Landstreet 1987). Analytical estimates predict appreciable field decay only after $\sim 10^{10}$–10^{11} yr, which exceeds the main sequence lifetime of even the least massive magnetic CP stars. Consequently, any observation of the possible secular evolution of magnetic field was often considered as a challenge for the fossil field theory. However, this classical assessment may be fundamentally flawed due to neglect of the toroidal field component, which must exist in the interior of magnetic CP stars in order to ensure dynamical stability of their global fields (Prendergast 1956; Tayler 1980). Recent numerical MHD simulations of the fossil field dynamics in radiative stellar interiors by Braithwaite & Spruit (2004, see also Braithwaite & Nordlund 2005) have established that instability of the poloidal field component can be suppressed by the presence of the interior toroidal magnetic component of similar strength. The diffusive evolution of such twisted fields in the simulations by Braithwaite & Nordlund (2005) is determined essentially by the toroidal field. In their model the total magnetic energy decreases with time, but the surface field strength is expected to increase, until the toroidal component emerges at the surface and the field decays rapidly. The time scale of this process is $\sim 2 \times 10^9$ yr for a $2\,M_\odot$ star (Braithwaite & Nordlund 2005), but the precise value is rather uncertain due to a very schematic treatment of the atmospheric magnetic reconnection and because of the sensitivity to the assumed initial field structure. These difficulties notwithstanding, the recent numerical work has emphasized limitations of the traditional analytical studies of the global field evolution and suggested that an observation of the long-term systematic change of the surface field is not necessarily incompatible with the fossil field hypothesis. Our observation of the uneven distribution of the low mass magnetic CP stars in the H-R diagram and of the possible increase in their surface magnetic flux with time may be plausibly interpreted as a signature of the Ohmic diffusion of the twisted fossil field. The relative shortage of the old low mass stars may indicate that in these objects we are observing the final stage of the field emergence and rapid decay. If this scenario is correct, the field starts to emerge in stars with $M \lesssim 2\,M_\odot$ after $\sim 4 \times 10^8$ yr of the main sequence evolution and completes its decay after $\sim 10^9$ yr.

The difference in the age distribution and magnetic field properties of the low and high mass CP stars may be related to their pre-main sequence (PMS) evolutionary history and, especially, to the behaviour of the interior and envelope convective zones. One can argue (e.g., Tout et al. 2004) that a large-scale coherent field typical of magnetic CP stars can be frozen in, or undergo a slow diffusive evolution as envisaged by Braithwaite & Nordlund (2005), in the fully radiative parts of the stellar interiors. In contrast, the turbulence in the convective zones leads to rapid reconnection of the field lines and thus contributes to the dissipation of the magnetic flux. Consequently, primordial field can survive only in stars that do not pass through a long fully convective phase during their approach to the ZAMS and in the subsequent main sequence evolution. Theoretical calculations of the PMS stellar evolution by Palla & Stahler (1993) have shown that, although the low mass stars are fully convective during a large fraction of their PMS life, the duration of this phase decreases rapidly with an increasing stellar mass. A $1.5\,M_\odot$ star is expected to spend roughly 10^5 years in the fully convective phase, which is already a factor of ten shorter compared to a solar-type star and is probably too short to destroy the fossil magnetic field completely. For masses of $\gtrsim 2.4\,M_\odot$ the PMS star is never fully convective, which facilitates survival of the primordial field. Thus, the observed difference in the age distribution of the low and high mass magnetic CP stars may reflect the history of the field dissipation in the convectively unstable regions of stellar interior. The presence of more extended and long-lived PMS convective zones in stars with $M \lesssim 2.4 - 2.0\,M_\odot$ suggests that these objects are more likely to possess weak or no field in the outer regions when they reach the ZAMS. Subsequent increase in the field strength results from the outward expansion of magnetic field into the newly formed radiative regions. In contrast to this scenario of

the field behaviour in the low mass stars, the fossil field in more massive magnetic CP stars is probably not significantly altered by the feeble PMS convective zones and appears close to the stellar surface even in young stars.

In the context of the study of the origin and evolution of the magnetic field in CP stars it is helpful also to investigate the evolution of the stellar angular momentum. Magnetic CP stars have generally longer rotation periods than normal A and B stars. The bulk of their rotation rates forms a separate Maxwellian distribution with an average value 3–4 times lower than that found in normal A and B-type stars (Stępień 2000), but there are also groups of CP stars with rotation period of years (Mathys et al. 1997) or decades (e.g., γ Equ, see Leroy et al. 1994). Several works suggest that neither field CP stars nor cluster CP stars undergo any significant magnetic braking during their life on the main sequence (North 1998; this study). Therefore, angular momentum must be lost before the star reaches the ZAMS. Stępień (2000) explains the slow rotation as the result of an interaction of the stellar magnetic field with the circumstellar environment during the PMS phase. And if a magnetised wind still persists after the dissipation of the circumstellar disk, a PMS CP star may further slow down, reaching the ZAMS with an extremely long rotation period. In this respect, the very existence of slow rotating stars with strong magnetic fields suggests that magnetic field was already present when the stars were in the pre-main sequence phase. For stars with $M > 2\,M_\odot$ this hypothesis is supported by the discovery of a magnetic field in NGC 2244 334, a 4 $M_\odot$ star that has spent only 2 % of its life in the main sequence (Bagnulo et al. 2004), and in HD 66318, a star with a mass of 2.1 $M_\odot$ and $\tau = 0.16$, that belongs to the open cluster NGC 2516. More direct confirmation that magnetic fields are present during the pre-main sequence phase comes from the discovery of magnetic field in Herbig Ae/Be stars (considered the progenitors of main sequence early-type stars) by Wade et al. (2005).

The most puzzling evolutionary properties are observed for the group of stars with $M \leq 2\,M_\odot$, which contains very few young stars and no stars approaching the terminal age main sequence. Observational evidence for lack of young lower mass ($M \lesssim 2\,M_\odot$) Ap stars comes also from open cluster studies. Abt (1979) suggested that low-mass Ap stars are found only in clusters that are at least 10^8 yr old, and a study of four nearby young clusters by Pöhnl et al. (2003) is also consistent with this finding. Assuming that magnetic breaking during pre-main sequence phase is the reason why these stars rotate slower than normal late A-type stars, then we face a scenario in which magnetic field appears and disappears from the stellar surface several times during the star life. Magnetic field was present at the surface of the star during the pre-main sequence phase, then disappeared when the star reached the ZAMS, to appear again at a more evolved state, and disappear toward the end of the star's life in the main sequence. At the same time, one can argue that magnetic field responsible for the PMS angular momentum loss is not directly related to the fossil field seen at the surfaces of main sequence low mass magnetic CP stars. The former field may be generated by the dynamo processes or represent the outer part of the fossil field tangled by the envelope convection. This complex field decays by the time the star reaches the ZAMS and, after some evolution on the main sequence, the interior fossil field which has retained its global organisation appears at the surface.

Our study is the first investigation which included enough very low mass magnetic CP stars to identify interesting characteristics of this stellar group, yet it is clear that the number of stars in the corresponding mass range is still rather small. This circumstance does not permit us to draw definite conclusions about the nature of the anomalies in the age distribution observed for these stars. Thus, we call for a more detailed analysis of the rotation, magnetic, and evolutionary characteristics of CP stars with $M \leq 2\,M_\odot$. Such an investigation would represent the most interesting follow up of the present study.

Acknowledgements. This research has made extensive use of the SIMBAD database, operated at CDS, Strasbourg, France, and NASA's Astrophysics Data System Bibliographic Services. OK acknowledges funding from the Scientific Visitors Programme of ESO Chile. We acknowledge the use of ESO Science Archive Facility.

References

Abt, H. A. 1979, ApJ, 230, 485
Aurière, M., Silvester, J., Wade, G. A., et al. 2004, in *IAU Symposium No. 224, The A-star puzzle*, eds. J. Zverko, J. Žižňovský, S.J. Adelman, W.W. Weiss, Cambridge University Press, IAUS 224, 633
Aznar Cuadrado, R., Jordan, S., Napiwotzki, R., et al. 2004, A&A, 423, 1081
Babcock, H. W. 1958, ApJS, 3, 141
Bagnulo, S., Szeifert, T., Wade, G. A., Landstreet, J. D., & Mathys, G. 2002, A&A, 389, 191
Bagnulo, S., Landstreet, J. D., Lo Curto, G., Szeifert, T., & Wade, G. A. 2003, A&A, 403, 645
Bagnulo, S., Hensberge, H., Landstreet, J. D., Szeifert, T., & Wade, G. A. 2004, A&A, 416, 1149
Bagnulo, S., Landstreet, J. D., Mason, E., et al. 2005, A&A, submitted
Bessell, M. 2000, in *Encyclopedia of Astronomy and Astrophysics*, IOP Publishing Ltd and Nature Publishing Group, 1638
Borra, E. F., & Landstreet, J. D. 1980, ApJS, 42, 421
Borra, E. F., & Landstreet, J. D., & Thompson, I. 1983, ApJS, 53, 151
Braithwaite, J., & Spruit, H. C. 2004, Nature, 431, 819
Braithwaite, J., & Nordlund, Å 2005, A&A, submitted (astro-ph/0510316)
Bychkov, V. D., Bychkova, L. V., & Madej, J. 2003, A&A, 407, 631
Casini, R., & Landi Degl'Innocenti, E. 1994, A&A, 291, 668
Catalano, F. A., & Renson, P. 1998, A&AS, 127, 421
Cowley, C. R., Ryabchikova, T., Kupka, F., et al. 2000, MNRAS, 317, 299
Cramer, N. 1982, A&A, 112, 330
Cowling, T. G. 1945, MNRAS, 105, 166
El'kin, V. G., Kudryavtsev, D. O., & Romanyuk, I. I. 2003, Astron. Letters, 29, 400
Fitzpatrick, E. L. 1999, PASP, 111, 63
Flower, P. J. 1996, ApJ, 469, 355
Johnson, N. M. 2004, M. Sc. thesis, Royal Military College of Canada
Jordan, S., Werner, K., & O'Toole, S. J. 2005, A&A, 432, 273
Golay, M. 1972, Vistas in Astron., 14, 13
Gomez, A.E., Luri, X., Grenier, S., et al. 1998, A&A, 336, 953
Hakkila, J., Myers, J. M., Stidham, B. J., & Hartmann, D. H. 1997, AJ, 114, 2043
Hauck, B., & Künzli, M. 1996, Baltic Astron., 5, 303

Hauck, B., & Mermilliod, M. 1998, A&AS, 129, 431
Hauck, B., & North, P. 1993, A&A, 269, 403
Hubrig, S., & Castelli, F. 2001, A&A, 375, 963
Hubrig, S., North, P., & Mathys, G. 2000, ApJ, 539, 352
Hubrig, S., Szeifert, T., Schöller, M., Mathys, G., & Kurtz, D. W. 2004, A&A, 415, 685
Hubrig, S., Nesvacil, N., Schöller, M., et al. 2005, A&A, 2005, A&A, 440, L37
Kochukhov, O., Bagnulo, S., & Barklem, P. S. 2002, ApJ, 578, L75
Koen, C., & Eyer, L. 2002, MNRAS, 331, 45
Künzli, M., North, P., Kurucz, R. L., & Nicolet, B. 1997, A&AS, 122, 51
Landstreet, J. D. 1987, MNRAS, 225, 437
Lanz, T. 1984, A&A, 139, 161
Leckrone, D. S. 1973, ApJ, 185, 577
Leroy, J. L., Bagnulo, S., Landolfi, M., & Landi Degl'Innocenti, E., 1994, A&A, 284, 174
Lucke, P. B. 1978, A&A, 64, 367
Lutz, T. E, & Kelker, D. H. 1973, PASP, 85, 573
Mathys, G. 1991, A&AS, 89, 121
Mathys, G., Hubrig, S., Landstreet, J. D., Lanz, T., & Manfroid, J. 1997, A&AS, 123, 353
Mathys, G., & Lanz, T. 1990, A&A, 230, L21
Moon, T. T., & Dworetsky, M. M. 1985, MNRAS, 217, 305
Moss, D. 1989, MNRAS, 236, 629
Moss, D. 1984, MNRAS, 207, 107
Moss, D. 2004, in *IAU Symposium No. 224, The A-star puzzle*, eds. J. Zverko, J. Žižňovský, S.J. Adelman, W.W. Weiss, Cambridge University Press, IAUS 224, 245
North, P. 1981, A&A, 97, 359
North, P. 1998, A&A, 334, 181
O'Toole, S. J., Jordan, S., Friedrich, S., & Heber, U. 2005, A&A, 437, 227
Palla, F., & Stahler, S. W. 1993, ApJ, 418, 414
Paunzen, E., & Maitzen, H. M. 1998, A&AS, 133, 1
Perryman, M. A. C., Lindegren, L., Kovalevsky, J., et al. 1997, A&AS, 323, 49
Pöhnl, H., Maitzen, H. M., & Paunzen, E. 2003, A&A, 402, 247
Pöhnl, H., Paunzen, E., & Maitzen, H. M. 2005, A&A, 441, 1111
Prendergast, K. H. 1956, ApJ, 123, 498
Press, W. H., Teukolsky, S. A., Vetterling, W. T., & Flannery, B. P. 1992, Numerical Recipes in FORTRAN. The Art of Scientific Computing, 2nd edn. Cambridge Univ. Press, Cambridge
Renson, P., Gerbaldi, M., & Catalano, F.A. 1991, A&AS, 89, 429
Romanyuk, I. I. 2000, in *Magnetic Fields of Chemically Peculiar and Related Stars*, eds. Yu.V. Glagolevskij and I.I. Romanyuk, Moscow, 18
Ryabchikova, T., Leone, F., Kochukhov, O., Bagnulo, S. 2004, in *IAU Symposium No. 224, The A-star puzzle*, eds. J. Zverko, J. Žižňovský, S.J. Adelman, W.W. Weiss, Cambridge University Press, IAUS 224, 580
Ryabchikova, T., Wade, G. A., Aurière, M., et al. 2005, A&A, 429, L55
Rufener, F. 1989, A&AS, 78, 469
Schaller, G., Schaerer, D., Meynet, G., & Maeder, A. 1992, A&AS, 96, 269
Schaerer, D., Charbonnel, C., Meynet, G., Maeder, A., & Schaller, G. 1993, A&AS, 102, 339
Schlegel, D. J., Finkbeiner, D. P., & Davis, M. 1998, ApJ, 500, 525
Shorlin, S. L. S., Wade, G. A., Donati, J.-F., et al. 2002, A&A, 392, 637
Smith, H. J. 2003, MNRAS, 338, 891
Sofia, U. J., & Meyer, D. M. 2001, ApJ, 588, L147
Stępień, K. 2000, A&A353, 227
Stępień, K. 2004, in *Magnetic Stars*, eds. Yu.V. Glagolevskij, D.O. Kudryavtsev, I.I. Romanyuk, Niznij Arkhyz, 19
Stütz, Ch., Ryabchikova, T., & Weiss, W. W. 2003, A&A, 402, 729
Tayler, R. J. 1980, MNRAS, 191, 151
Tout, C. A., Wikramasinghe, D. T., & Ferrario, L. 2004, MNRAS, 355, L13
van Leeuwen, F., & Fantino, E. 2005, A&A, 439, 791
Wade, G. A., Aurière, M., Donati, J.-F., et al. 2003, in *IAU Symposium No. 210, Modelling of Stellar Atmospheres*, eds. N.E. Piskunov, W.W. Weiss, D.F. Gray, ASP, D29
Wade, G.A., Drouin, D., Bagnulo, S., et al. 2005, A&A, 442, L31

Online Material

Table 1. $\langle B_z \rangle$ measurements for the sample of CP stars observed with FORS1 (data retrieved from the ESO archive). Columns 1 and 2 list the HD and HIP identification. Columns 3 and 4 give the *V*-magnitude and spectral type, respectively, most of which are extracted from the *General catalogue of Ap and Am stars* by Renson et al. (1991). Column 5 gives the Julian Date of the middle of the exposures. Column 6 reports $\langle B_z \rangle$ with its error bar in Gauss. The last column indicates stars for which magnetic field was detected for the first time (new detection, ND) or confirmed (confirmed detection, CD).

HD	HIP	*V*	Sp. Type	JD	$\langle B_z \rangle$ (G)	Comment
1048	1193	6.2	A1 Si	2452910.603	403±105	ND
				2453199.906	−89± 46	
				2453215.882	36± 45	
3326	2852	6.1	A6 Sr	2452908.690	99± 62	
8783	6534	7.8	A2 Sr Cr Eu	2452852.858	−29±106	
10840	8132	6.8	B9 Si	2453184.831	−148± 81	
19712	14736	7.3	A0 Cr Eu	2452905.884	−930±109	ND
				2452999.525	764± 66	
19918	14026	9.4	A5 Sr Cr Eu	2452908.711	−777±109	ND
22374	16859	6.7	A1 Cr Sr Si	2452999.538	−10± 64	
				2453216.880	63± 36	
22488	16527	7.7	A3 Sr Cr Eu	2453087.514	114± 51	
23207	17345	7.5	A2 Sr Eu	2453215.861	259± 72	ND
				2453218.835	394± 53	
23408	17573	3.9	B7 He-weak Mn	2452963.656	24± 65	
24188	17543	6.3	A0 Si	2453087.532	426± 48	ND
30612	21949	5.5	B9 Si	2453087.546	44± 44	
34797	24827	6.5	B8 He-weak Si	2452999.566	1059± 86	ND
42659	29365	6.7	A3 Sr Cr Eu	2452999.619	418± 78	ND
55522	34798	5.9	B2 Si He	2452999.699	168± 81	
				2453000.553	821± 68	ND
56350	34929	6.7	A0 Sr Cr Eu	2452999.739	824± 86	ND
56455	35029	5.7	A0 Si	2452999.751	85± 98	
58448	35676	7.1	B8 Si	2452999.765	60± 99	
60435	36537	8.9	A3 Sr Eu	2453000.572	−315± 87	ND
63401	37982	6.3	B9 Si	2453002.553	48±113	
				2453004.728	−486±106	ND
74168	42519	7.5	B9 Si	2453002.611	−75± 76	
74196	42535	5.6	B7 He-weak	2452906.888	121±122	
75989	43528	6.5	B9 Si	2452992.841	−279±161	
				2453004.783	−46±102	
80316	45658	7.8	A3 Sr Eu	2452992.857	−269±134	
83625	47272	6.9	A0 Si Sr	2453008.822	−1484± 83	ND
84041		9.4	A5 Sr Eu	2453002.670	497± 91	ND
86181	48619	9.4	F0 Sr	2453002.692	360± 77	ND
86199	48643	6.7	B9 Si	2453003.845	−768± 89	ND
88158	49642	6.5	B8 Si	2453008.838	233± 77	ND
88385	49791	8.1	A0 Si Cr Eu	2453010.681	−958± 70	ND
89103	50248	7.8	B9 Si	2453010.702	−1949± 84	ND
89385	50398	8.4	B9 Si Cr Eu	2453010.718	−81± 87	
91239	51512	7.4	B9 Si Cr Eu	2453118.559	−116± 77	
92106	51632	7.8	A0 Sr Cr Eu	2453010.739	72± 98	
				2453118.580	−89± 90	
92385	52059	6.7	B9 Si	2453008.869	−588± 90	ND
				2453020.832	240±101	
92499	52218	8.9	A2 Sr Cr Eu	2453010.755	−1163±324	ND
				2453011.712	−1230±124	
				2453118.595	−989±141	
93030	52419	2.7	B0 Si N P	2453012.731	−46±132	
96451	54166	6.9	A0 Sr	2453074.840	1± 51	
98340	55181	7.1	B9 Si	2453074.862	1033± 65	ND
99563	55890	8.5	F0 Sr	2453012.747	−392±124	CD
				2453015.725	−669±159	
105379	59167	8.0	A0 Sr Cr	2453011.750	25± 83	
105382	59173	4.5	B6 He	2453011.695	−1000±101	ND

Table 1. Continued.

HD	HIP	V	Sp. Type	JD	$\langle B_z \rangle$ (G)	Comment
				2453015.746	−610±136	
105770	59404	7.4	B9 Si	2453011.733	449±110	ND
				2453120.645	262± 71	
105999	59487	7.4	F1 Sr Cr	2453011.770	−30±128	
107696	60379	5.4	B8 Cr	2452824.530	−46±108	
				2453074.875	−75±142	
108945	61071	5.5	A3 Sr	2453015.835	65±116	
114365	64320	6.1	A0 Si	2452824.543	8±100	
115226	64883	8.5	A3 Sr	2453086.799	677± 57	ND
115440	65053	8.2	B9 Si	2453077.714	3217± 61	ND
116890	65755	6.2	B9 Si	2452824.555	−292± 77	ND
117025	65783	6.1	A2 Sr Cr Eu	2452824.567	483± 84	ND
				2453120.664	463± 68	
118913	66888	7.7	A0 Sr Cr Eu	2452824.581	−345± 88	ND
				2453120.681	−555± 38	
119308	66942	7.8	A0 Sr Cr Eu	2453120.704	−326± 61	ND
122970	68790	8.3	F0 Sr Cr Eu	2453015.850	526±137	CD
125630	70346	6.8	A2 Si Cr Sr	2452824.607	660± 67	ND
				2453120.721	30± 55	
127453	71314	7.4	B8 Si	2452824.621	−361± 85	ND
127575	71359	7.7	B9 Si	2453079.888	911± 64	ND
128775	71727	6.6	B9 Si	2453120.736	−278± 52	ND
128974	71783	5.7	A0 Si	2452824.644	−43± 55	
129899	72670	6.4	A0 Si	2453120.795	495± 42	ND
130158	72323	5.6	B9 Si	2452824.676	2± 53	
				2453116.812	9± 45	
130557	72449	6.1	B9 Si Cr	2452853.558	−10± 70	
				2453144.767	19± 43	
131120	72800	5.0	B7 He-weak	2452824.660	−152±114	
				2453020.857	57± 77	
				2453030.864	152±125	
132322	73520	7.4	A7 Sr Cr Eu	2453111.811	340± 40	ND
133792	74181	6.3	A0 Sr Cr	2452853.570	119± 77	CD
				2453120.812	124± 40	
134305	74109	7.2	A6 Sr Cr Eu	2453144.801	170± 49	ND
136933	75439	5.4	A0 Si	2452823.720	23± 89	
138758	76767	7.9	B9 Si	2453086.828	430± 41	ND
138764	76243	5.2	B6 Si	2452904.515	202± 95	
138769	76371	4.5	B3 He	2452904.503	91± 95	
				2452904.527	123± 91	
				2452908.522	−166±120	
145102	79235	6.6	B9 Si	2452763.815	40± 79	
147869	80351	5.8	A1 Sr	2452763.827	53± 74	
				2453144.818	7± 40	
148112	80463	4.6	A0 Cr Eu	2452763.838	−59± 64	
148898	80975	4.4	A6 Sr Cr Eu	2452763.849	241± 84	
149764	81477	6.9	A0 Si	2452763.874	−1169± 86	ND
				2453120.831	49± 48	
149822	81337	6.4	B9 Si Cr	2452763.861	−657± 66	ND
150549	82129	5.1	A0 Si	2452763.886	−167± 63	
				2453116.886	−52± 60	
				2453120.850	−49± 34	
151525	82216	5.2	B9 Eu Cr	2452733.895	76± 73	
				2452763.897	237± 75	CD
154708	84017	8.8	A2 Sr Cr Eu	2453120.876	6859± 58	CD
157751	85372	7.6	B9 Si Cr	2452793.771	4070± 65	ND
				2453116.904	3982± 48	
160468	86930	7.3	F2 Sr Cr	2453116.862	−96± 83	
				2453134.819	−55± 54	
161277	86983	7.1	B9 Si	2453134.840	94± 44	

Table 1. Continued.

HD	HIP	V	Sp. Type	JD	$\langle B_z \rangle$ (G)	Comment
166469	89178	6.5	A0 Si Cr Sr	2452793.791	−42± 49	
				2453136.772	−26± 45	
168856	90030	7.0	B9 Si	2453144.840	−530± 59	ND
171184	91001	8.0	A0 Si	2452880.529	250± 52	ND
				2453144.868	−14± 48	
171279	91031	7.3	A0 Sr Cr Eu	2453144.893	−40± 40	
172032	91414	7.7	A9 Sr Cr	2453151.605	−31± 55	
172690	93481	7.5	A0 Si Sr Cr	2452793.814	−287± 86	ND
				2453134.868	235± 52	
175744	92934	6.6	B9 Si	2452880.555	104± 76	
				2452901.519	162± 91	
176196	93863	7.5	B9 Eu Cr	2452793.829	240± 83	ND
				2453134.889	190± 51	
183806	96178	5.6	A0 Cr Eu Sr	2452793.845	−23± 64	ND
				2453120.924	148± 37	
186117	97533	7.3	A0 Sr Cr Eu	2453134.913	−19± 49	
				2453140.829	27± 46	
192674	100090	7.5	B9 Cr Eu Sr	2453137.861	7± 44	
199180	103246	7.7	A0 Si Cr	2452822.844	−228± 85	
199728	103616	6.2	B9 Si	2452822.857	−245± 73	ND
201018	104337	8.6	A2 Cr Eu	2453151.871	546± 43	ND
202627	105140	4.7	A1 Si	2452793.874	−56± 68	
206653	107525	7.2	B9 Si	2452793.894	32± 68	
212385	110624	6.8	A3 Sr Cr Eu	2452822.913	163± 72	ND
				2453184.797	626± 52	
221760	116389	4.7	A2 Sr Cr Eu	2452793.915	−48± 97	
				2453184.814	62± 65	

Table 2. Fundamental parameters of magnetic CP stars. The columns give numbers in the HD and Hipparcos catalogues, distance determined from the Hipparcos parallax, absolute magnitude, $T_{\rm eff}$, luminosity and mass in solar units, absolute and fractional stellar age. For the last two columns numbers in brackets give 1σ ranges compatible with the errors of $T_{\rm eff}$ and $L/L_\odot$.

HD	HIP	d (pc)	M_V	log $T_{\rm eff}$ (K)	log $L/L_\odot$	$M/M_\odot$	log t (yr)	τ
1048	1193	108±8	1.05±0.17	3.949±0.015	1.50±0.07	2.17±0.06	8.72 (8.63−8.79)	0.61 (0.49−0.71)
2453	2243	151±18	0.88±0.27	3.949±0.015	1.57±0.11	2.24±0.10	8.72 (8.65−8.78)	0.68 (0.54−0.78)
3980	3277	65±2	1.62±0.09	3.917±0.011	1.24±0.04	1.91±0.03	8.83 (8.75−8.89)	0.53 (0.45−0.61)
4778	3919	90±6	1.23±0.15	3.999±0.013	1.51±0.07	2.29±0.06	8.26 (7.53−8.47)	0.24 (0.03−0.40)
5737	4577	206±35	−2.31±0.38	4.121±0.013	3.19±0.15	5.01±0.21	7.97 (7.92−8.01)	1.00 (1.00−1.00)
8441	6560	203±33	0.17±0.35	3.956±0.014	1.86±0.14	2.57±0.18	8.66 (8.61−8.71)	0.85 (0.76−0.93)
9996	7651	139±16	0.80±0.26	4.012±0.013	1.70±0.11	2.50±0.10	8.41 (8.16−8.51)	0.44 (0.23−0.60)
10221	7965	136±11	−0.21±0.18	4.030±0.016	2.15±0.08	3.05±0.11	8.42 (8.37−8.46)	0.79 (0.69−0.86)
10783	8210	186±25	0.08±0.30	4.006±0.013	1.98±0.12	2.79±0.15	8.51 (8.47−8.55)	0.76 (0.65−0.85)
11187	8643	234±44	0.14±0.41	4.029±0.016	2.00±0.17	2.87±0.20	8.43 (8.33−8.49)	0.68 (0.48−0.82)
11503	8832	62±3	0.60±0.12	4.010±0.013	1.78±0.05	2.57±0.06	8.47 (8.38−8.54)	0.55 (0.44−0.65)
12288	9604	230±38	0.59±0.36	3.996±0.013	1.75±0.15	2.51±0.15	8.54 (8.42−8.60)	0.61 (0.42−0.75)
12447	9487	42±1	1.03±0.10	3.999±0.013	1.58±0.05	2.36±0.05	8.41 (8.21−8.53)	0.37 (0.23−0.49)
12767	9677	110±9	−0.56±0.19	4.111±0.013	2.47±0.08	3.75±0.13	8.13 (8.07−8.18)	0.70 (0.59−0.79)
14437	10951	197±36	0.51±0.40	4.034±0.016	1.87±0.16	2.72±0.17	8.36 (8.03−8.46)	0.50 (0.21−0.69)
15089	11569	43±1	1.46±0.08	3.925±0.010	1.31±0.03	1.97±0.03	8.80 (8.74−8.86)	0.56 (0.48−0.62)
15144	11348	65±4	1.91±0.14	3.926±0.010	1.13±0.06	1.84±0.04	8.63 (8.30−8.77)	0.30 (0.13−0.42)
17775	13507	156±23	1.92±0.33	3.930±0.015	1.13±0.13	1.85±0.09	8.57 (7.05−8.81)	0.26 (0.00−0.50)
18296	13775	118±12	−0.44±0.23	4.036±0.016	2.25±0.10	3.21±0.15	8.38 (8.34−8.43)	0.83 (0.74−0.90)
18610	13534	202±27	1.55±0.30	3.878±0.012	1.27±0.12	1.88±0.11	9.00 (8.96−9.04)	0.76 (0.65−0.84)
19712	14376	166±25	1.16±0.33	4.056±0.015	1.66±0.14	2.61±0.11	6.74 (6.65−8.04)	0.00 (0.00−0.22)
19805	14980	168±24	1.41±0.32	3.973±0.014	1.39±0.13	2.13±0.10	8.43 (7.05−8.63)	0.29 (0.00−0.51)
19832	14893	113±11	0.35±0.22	4.095±0.014	2.07±0.09	3.17±0.12	7.95 (7.33−8.16)	0.29 (0.06−0.49)
21699	16470	179±22	−1.05±0.28	4.159±0.012	2.78±0.12	4.48±0.22	7.96 (7.91−8.01)	0.74 (0.62−0.83)
22316	16974	170±20	0.04±0.26	4.073±0.015	2.14±0.11	3.16±0.13	8.24 (8.09−8.32)	0.58 (0.39−0.71)
22374	16859	134±17	0.82±0.28	3.938±0.015	1.58±0.11	2.24±0.12	8.76 (8.71−8.81)	0.74 (0.62−0.83)
22470	16803	145±17	−0.38±0.26	4.115±0.013	2.41±0.11	3.67±0.15	8.10 (7.99−8.16)	0.62 (0.46−0.74)
22920	17167	226±38	−1.32±0.37	4.142±0.013	2.85±0.15	4.54±0.32	8.01 (7.96−8.05)	0.85 (0.74−0.93)
23207	17345	177±31	1.28±0.38	3.896±0.011	1.38±0.15	2.00±0.14	8.93 (8.87−8.97)	0.76 (0.64−0.85)
23408	17573	110±12	−1.54±0.25	4.079±0.014	2.79±0.10	4.22±0.18	8.15 (8.12−8.18)	0.97 (0.92−1.00)
24155	18033	135±16	0.32±0.27	4.132±0.013	2.17±0.11	3.45±0.14	7.30 (6.27−7.88)	0.08 (0.00−0.32)
24188	17543	142±10	0.40±0.17	4.101±0.014	2.06±0.07	3.19±0.10	7.81 (6.67−8.07)	0.21 (0.01−0.40)
24712	18339	48±2	2.54±0.09	3.857±0.012	0.87±0.04	1.55±0.03	9.07 (8.94−9.17)	0.50 (0.37−0.61)
25267	18673	101±7	−0.30±0.15	4.080±0.014	2.30±0.07	3.38±0.10	8.24 (8.18−8.29)	0.70 (0.59−0.78)
25354	18912	144±20	1.79±0.31	3.993±0.013	1.27±0.13	2.12±0.08	7.05 (7.02−8.05)	0.00 (0.00−0.11)
25823	19171	151±19	−0.63±0.28	4.112±0.013	2.50±0.12	3.80±0.19	8.13 (8.07−8.17)	0.72 (0.59−0.82)
27309	20186	96±7	0.40±0.16	4.079±0.014	2.01±0.07	3.04±0.09	8.07 (7.73−8.23)	0.34 (0.15−0.51)
28843	21192	131±14	0.06±0.24	4.143±0.013	2.30±0.10	3.67±0.14	7.65 (6.26−7.93)	0.21 (0.00−0.43)
30466	22402	163±25	0.68±0.34	4.044±0.016	1.82±0.14	2.71±0.14	8.21 (7.40−8.40)	0.34 (0.04−0.57)
32633	23733	156±22	0.72±0.32	4.108±0.014	1.95±0.13	3.10±0.13	6.39 (6.33−7.82)	0.00 (0.00−0.21)
34452	24799	137±13	−0.33±0.21	4.160±0.012	2.49±0.09	4.02±0.14	7.82 (7.51−7.94)	0.40 (0.19−0.55)
34797	24827	238±47	−0.47±0.43	4.102±0.014	2.41±0.17	3.62±0.26	8.16 (8.05−8.21)	0.69 (0.49−0.82)
38823	27423	113±12	2.00±0.24	3.839±0.013	1.09±0.10	1.70±0.08	9.16 (9.11−9.21)	0.80 (0.71−0.88)
39317	27743	157±22	−0.50±0.31	4.018±0.013	2.24±0.13	3.16±0.19	8.42 (8.37−8.47)	0.88 (0.80−0.93)
40312	28380	53±2	−1.01±0.10	4.007±0.013	2.42±0.05	3.41±0.07	8.36 (8.34−8.39)	1.00 (0.94−1.00)
42616	29565	173±28	0.56±0.35	3.989±0.013	1.76±0.14	2.50±0.15	8.57 (8.49−8.62)	0.65 (0.48−0.77)
42659	29365	135±14	1.03±0.23	3.900±0.011	1.48±0.09	2.10±0.10	8.88 (8.85−8.92)	0.81 (0.74−0.87)
49333	32504	204±30	−0.51±0.32	4.216±0.013	2.69±0.13	4.71±0.23	7.27 (6.07−7.67)	0.16 (0.00−0.43)
49976	32838	101±8	1.20±0.18	3.984±0.014	1.49±0.07	2.24±0.07	8.45 (8.14−8.59)	0.35 (0.16−0.51)
54118	34105	86±3	0.38±0.09	4.022±0.017	1.89±0.05	2.72±0.07	8.45 (8.34−8.52)	0.61 (0.49−0.70)
55522	34798	220±29	−0.87±0.29	4.211±0.013	2.82±0.12	4.88±0.22	7.67 (7.36−7.79)	0.46 (0.21−0.64)
55719	34802	133±8	0.37±0.14	3.960±0.014	1.79±0.06	2.49±0.07	8.67 (8.63−8.70)	0.80 (0.73−0.85)
56350	34929	161±12	0.64±0.18	4.022±0.017	1.79±0.08	2.61±0.09	8.40 (8.19−8.51)	0.48 (0.29−0.62)
60435	36537	233±45	1.87±0.43	3.910±0.011	1.14±0.17	1.82±0.12	8.82 (8.36−8.91)	0.46 (0.12−0.65)
62140	37934	81±4	1.89±0.13	3.884±0.011	1.13±0.05	1.77±0.04	8.99 (8.93−9.04)	0.62 (0.53−0.69)
63401	37982	210±24	−0.40±0.26	4.129±0.013	2.45±0.11	3.79±0.16	8.03 (7.90−8.11)	0.58 (0.41−0.71)
64486	39538	101±5	0.32±0.12	3.999±0.013	1.87±0.05	2.65±0.06	8.54 (8.49−8.59)	0.70 (0.62−0.77)

Table 2. Continued.

HD	HIP	d (pc)	M_V	log $T_{\rm eff}$ (K)	log $L/L_\odot$	$M/M_\odot$	log t (yr)	τ
64740	38500	220±25	−2.15±0.25	4.353±0.010	3.63±0.10	8.30±0.30	7.10 (6.79−7.24)	0.40 (0.18−0.57)
65339	39261	98±7	1.12±0.17	3.919±0.010	1.45±0.07	2.08±0.06	8.84 (8.81−8.87)	0.72 (0.64−0.78)
71866	41782	146±18	0.83±0.28	3.944±0.015	1.58±0.11	2.24±0.11	8.74 (8.68−8.79)	0.71 (0.58−0.81)
72968	42146	82±5	1.11±0.15	3.992±0.013	1.54±0.07	2.30±0.06	8.43 (8.18−8.55)	0.36 (0.19−0.50)
73340	42177	143±9	−0.10±0.14	4.145±0.012	2.37±0.06	3.77±0.11	7.79 (7.45−7.95)	0.32 (0.14−0.47)
74521	42917	125±13	0.07±0.23	4.033±0.016	2.04±0.10	2.92±0.12	8.42 (8.35−8.47)	0.69 (0.56−0.79)
75445	43257	113±8	1.79±0.16	3.885±0.011	1.17±0.06	1.80±0.05	8.99 (8.93−9.03)	0.65 (0.56−0.72)
79158	45290	175±25	−0.94±0.31	4.097±0.014	2.59±0.13	3.91±0.23	8.16 (8.12−8.20)	0.84 (0.74−0.92)
81009	45999	138±15	1.17±0.24	3.900±0.011	1.42±0.10	2.04±0.09	8.90 (8.86−8.94)	0.78 (0.69−0.84)
83368	47145	72±3	1.91±0.12	3.877±0.012	1.12±0.05	1.76±0.04	9.02 (8.96−9.07)	0.65 (0.56−0.72)
83625	47272	191±23	0.35±0.26	4.082±0.014	2.04±0.11	3.08±0.12	8.07 (7.63−8.24)	0.36 (0.12−0.56)
86199	48643	235±28	−0.27±0.27	4.112±0.013	2.36±0.11	3.58±0.15	8.10 (7.95−8.16)	0.58 (0.40−0.71)
88158	49642	250±32	−0.72±0.28	4.113±0.013	2.54±0.12	3.87±0.20	8.12 (8.08−8.16)	0.75 (0.63−0.84)
88385	49791	273±47	0.66±0.38	4.030±0.016	1.80±0.16	2.64±0.15	8.34 (7.88−8.47)	0.43 (0.13−0.64)
89103	50248	203±27	1.19±0.29	4.069±0.015	1.67±0.12	2.68±0.11	6.68 (6.59−7.64)	0.00 (0.00−0.08)
90044	50885	107±8	0.74±0.17	4.002±0.013	1.71±0.07	2.48±0.07	8.49 (8.36−8.56)	0.52 (0.38−0.63)
90569	51213	118±11	0.64±0.21	4.003±0.013	1.75±0.09	2.52±0.09	8.50 (8.39−8.57)	0.56 (0.42−0.68)
92385	52059	147±12	0.81±0.18	4.043±0.016	1.77±0.08	2.66±0.09	8.12 (7.28−8.35)	0.26 (0.03−0.46)
92499	52218	224±44	2.10±0.44	3.858±0.012	1.05±0.17	1.68±0.13	9.10 (9.02−9.14)	0.68 (0.49−0.81)
92664	52221	142±10	−0.32±0.16	4.155±0.012	2.48±0.07	3.97±0.12	7.84 (7.62−7.96)	0.41 (0.24−0.55)
94427	53290	110±11	2.02±0.22	3.861±0.012	1.08±0.09	1.71±0.07	9.09 (9.04−9.13)	0.69 (0.59−0.78)
94660	53379	151±15	0.20±0.22	4.032±0.016	1.98±0.09	2.85±0.11	8.42 (8.33−8.48)	0.64 (0.50−0.75)
96707	54540	108±7	0.87±0.14	3.893±0.011	1.54±0.06	2.16±0.06	8.87 (8.84−8.90)	0.86 (0.82−0.90)
98088	55106	129±12	0.79±0.21	3.899±0.011	1.57±0.09	2.20±0.09	8.85 (8.81−8.89)	0.86 (0.81−0.91)
98340	55181	226±37	0.86±0.35	4.028±0.016	1.71±0.15	2.56±0.14	8.24 (6.82−8.45)	0.32 (0.00−0.56)
101065	56709	125±16	2.48±0.29	3.810±0.013	0.91±0.12	1.53±0.09	9.32 (9.25−9.40)	0.86 (0.76−0.94)
103192	57936	111±11	−0.57±0.21	4.044±0.016	2.32±0.09	3.33±0.14	8.34 (8.30−8.39)	0.85 (0.77−0.91)
105382	59173	115±9	−0.93±0.18	4.212±0.013	2.85±0.08	4.93±0.17	7.69 (7.49−7.78)	0.49 (0.31−0.62)
105770	59404	194±23	0.09±0.27	4.115±0.013	2.22±0.11	3.43±0.14	7.94 (7.49−8.11)	0.36 (0.12−0.55)
108662	60904	82±5	0.57±0.15	4.021±0.017	1.81±0.07	2.63±0.08	8.42 (8.26−8.52)	0.52 (0.35−0.65)
108945	61071	95±7	0.54±0.17	3.952±0.015	1.71±0.07	2.39±0.08	8.70 (8.66−8.74)	0.78 (0.69−0.84)
109026	61199	99±5	−1.28±0.12	4.173±0.012	2.90±0.05	4.79±0.12	7.91 (7.87−7.95)	0.78 (0.71−0.83)
110066	61748	155±17	0.41±0.25	3.947±0.015	1.75±0.10	2.44±0.12	8.71 (8.66−8.74)	0.82 (0.73−0.89)
111133	62376	160±23	0.20±0.33	3.997±0.013	1.92±0.13	2.69±0.16	8.55 (8.50−8.58)	0.75 (0.62−0.84)
112185	62956	24±0	−0.21±0.04	3.953±0.015	2.01±0.02	2.76±0.03	8.61 (8.59−8.63)	0.94 (0.90−0.97)
112381	63204	100±8	1.53±0.19	3.999±0.013	1.39±0.08	2.20±0.07	7.02 (6.98−8.26)	0.00 (0.00−0.22)
112413	63125	33±1	0.26±0.08	4.060±0.015	2.03±0.05	2.98±0.07	8.27 (8.14−8.36)	0.52 (0.39−0.63)
115226	64883	141±18	2.57±0.29	3.883±0.011	0.86±0.12	1.60±0.05	8.60 (7.37−9.16)	0.18 (0.00−0.62)
115440	65053	229±40	0.81±0.39	4.086±0.014	1.86±0.16	2.91±0.15	6.51 (6.45−8.04)	0.00 (0.00−0.30)
115708	64936	132±18	2.19±0.31	3.880±0.011	1.01±0.12	1.68±0.08	8.97 (8.76−9.04)	0.50 (0.28−0.65)
116114	65203	140±17	1.41±0.28	3.870±0.012	1.32±0.11	1.92±0.10	9.01 (8.96−9.05)	0.82 (0.74−0.89)
116458	65522	142±11	−0.15±0.18	4.012±0.013	2.08±0.07	2.93±0.10	8.48 (8.44−8.51)	0.81 (0.74−0.87)
116890	65755	214±26	−0.94±0.27	4.112±0.013	2.63±0.11	4.01±0.20	8.12 (8.08−8.15)	0.81 (0.72−0.89)
117025	65783	88±4	1.25±0.13	3.945±0.015	1.42±0.05	2.09±0.05	8.72 (8.61−8.80)	0.55 (0.43−0.65)
118022	66200	56±2	1.17±0.10	3.957±0.014	1.46±0.04	2.16±0.05	8.66 (8.56−8.74)	0.52 (0.41−0.62)
118913	66888	206±31	0.73±0.33	3.981±0.014	1.67±0.14	2.40±0.14	8.60 (8.48−8.66)	0.61 (0.43−0.74)
119213	66700	88±4	1.52±0.12	3.941±0.015	1.30±0.05	1.99±0.05	8.69 (8.51−8.80)	0.43 (0.29−0.55)
119308	66942	182±31	1.35±0.37	4.009±0.013	1.48±0.15	2.30±0.11	7.73 (6.93−8.40)	0.06 (0.00−0.36)
119419	67036	112±9	1.16±0.18	4.048±0.016	1.64±0.08	2.55±0.09	6.78 (6.71−8.05)	0.00 (0.00−0.20)
120198	67231	86±4	0.98±0.12	4.023±0.016	1.65±0.06	2.49±0.07	8.20 (7.59−8.41)	0.26 (0.06−0.43)
122532	68673	169±21	−0.15±0.28	4.071±0.015	2.22±0.12	3.25±0.15	8.27 (8.18−8.33)	0.67 (0.51−0.78)
122970	68790	129±16	2.74±0.28	3.840±0.013	0.79±0.11	1.48±0.07	9.20 (8.99−9.29)	0.57 (0.33−0.71)
124224	69389	80±5	0.46±0.16	4.084±0.014	2.00±0.07	3.04±0.09	7.97 (7.45−8.18)	0.27 (0.07−0.45)
125248	69929	90±7	1.20±0.18	3.992±0.013	1.50±0.08	2.27±0.07	8.37 (7.94−8.53)	0.30 (0.10−0.47)
125630	70346	159±16	0.55±0.23	3.966±0.014	1.72±0.10	2.42±0.10	8.66 (8.61−8.70)	0.73 (0.62−0.81)
125823	70300	128±12	−1.18±0.21	4.248±0.012	3.02±0.09	5.57±0.20	7.51 (7.25−7.63)	0.45 (0.24−0.59)
126515	70553	141±21	1.26±0.32	4.007±0.013	1.51±0.13	2.32±0.11	8.07 (6.93−8.44)	0.16 (0.00−0.41)
127453	71314	257±49	−0.17±0.42	4.083±0.014	2.25±0.17	3.33±0.23	8.22 (8.07−8.28)	0.64 (0.41−0.79)
127575	71359	183±28	0.91±0.34	4.081±0.014	1.81±0.14	2.84±0.13	6.55 (6.49−7.98)	0.00 (0.00−0.24)
128775	71727	161±22	0.48±0.30	4.076±0.015	1.97±0.12	2.98±0.13	8.04 (7.12−8.25)	0.30 (0.03−0.53)

Table 2. Continued.

HD	HIP	d (pc)	M_V	log $T_{\rm eff}$ (K)	log $L/L_\odot$	$M/M_\odot$	log t (yr)	τ
128898	71908	16±0	2.12±0.03	3.885±0.011	1.04±0.01	1.71±0.02	8.95 (8.86−9.03)	0.51 (0.42−0.58)
129899	72670	275±43	−0.94±0.34	4.017±0.013	2.41±0.14	3.43±0.19	8.36 (8.31−8.41)	0.95 (0.89−1.00)
130559	72489	72±6	1.32±0.20	3.957±0.014	1.40±0.08	2.10±0.07	8.62 (8.42−8.72)	0.44 (0.26−0.58)
132322	73520	173±21	0.93±0.28	3.922±0.010	1.52±0.11	2.16±0.11	8.82 (8.78−8.86)	0.76 (0.67−0.83)
133029	73454	146±11	0.48±0.18	4.027±0.016	1.86±0.08	2.70±0.09	8.41 (8.26−8.49)	0.54 (0.37−0.67)
133652	73937	95±8	0.81±0.20	4.113±0.013	1.93±0.09	3.10±0.10	6.39 (6.34−7.21)	0.00 (0.00−0.04)
133792	74181	170±19	−0.17±0.24	3.974±0.014	2.02±0.10	2.80±0.14	8.58 (8.54−8.62)	0.89 (0.82−0.94)
133880	74066	126±13	0.25±0.23	4.079±0.014	2.07±0.10	3.10±0.12	8.15 (7.88−8.27)	0.44 (0.22−0.60)
134214	74145	91±7	2.58±0.18	3.858±0.012	0.85±0.07	1.55±0.04	9.05 (8.84−9.16)	0.47 (0.28−0.61)
134305	74109	177±27	0.93±0.33	3.908±0.011	1.52±0.13	2.15±0.14	8.85 (8.80−8.90)	0.81 (0.72−0.88)
137509	76011	249±37	−0.28±0.33	4.147±0.012	2.44±0.14	3.88±0.18	7.89 (7.51−8.02)	0.43 (0.17−0.62)
137909	75695	34±0	1.12±0.06	3.871±0.012	1.44±0.02	2.04±0.02	8.95 (8.93−8.97)	0.88 (0.84−0.91)
137949	75848	89±6	1.80±0.17	3.861±0.012	1.16±0.07	1.78±0.06	9.07 (9.03−9.11)	0.75 (0.68−0.82)
138758	76767	238±44	0.92±0.41	4.023±0.016	1.68±0.17	2.51±0.15	8.26 (6.86−8.47)	0.31 (0.00−0.57)
140160	76866	70±4	1.04±0.13	3.968±0.014	1.53±0.06	2.24±0.06	8.62 (8.52−8.70)	0.53 (0.41−0.63)
140728	76957	97±4	0.51±0.11	4.021±0.012	1.84±0.05	2.66±0.06	8.43 (8.35−8.50)	0.55 (0.44−0.64)
142301	77909	139±23	−0.24±0.37	4.193±0.011	2.53±0.15	4.30±0.21	7.21 (6.14−7.72)	0.11 (0.00−0.40)
142990	78246	149±18	−0.74±0.27	4.217±0.013	2.78±0.11	4.87±0.20	7.54 (6.98−7.73)	0.34 (0.08−0.54)
143473	78533	123±15	1.06±0.27	4.109±0.014	1.82±0.11	3.00±0.12	6.44 (6.38−6.52)	0.00 (0.00−0.00)
144334	78877	149±19	−0.29±0.28	4.168±0.012	2.50±0.12	4.08±0.17	7.72 (7.10−7.90)	0.33 (0.07−0.52)
145501	79374	133±19	0.03±0.33	4.141±0.013	2.31±0.13	3.67±0.17	7.72 (6.26−7.98)	0.25 (0.00−0.50)
147010	80024	143±19	0.54±0.30	4.117±0.013	2.04±0.12	3.23±0.14	6.47 (6.30−7.86)	0.00 (0.00−0.27)
148112	80463	72±4	0.20±0.15	3.970±0.014	1.87±0.06	2.60±0.08	8.63 (8.59−8.66)	0.81 (0.75−0.87)
148199	80607	150±21	0.49±0.31	4.046±0.016	1.90±0.13	2.79±0.13	8.29 (7.95−8.40)	0.45 (0.20−0.64)
148330	80375	112±6	0.49±0.12	3.947±0.015	1.72±0.05	2.40±0.06	8.71 (8.67−8.74)	0.80 (0.74−0.85)
149764	81477	126±15	0.99±0.28	4.128±0.013	1.89±0.12	3.19±0.12	6.35 (6.31−6.41)	0.00 (0.00−0.00)
149822	81337	133±14	0.70±0.23	4.010±0.013	1.74±0.10	2.53±0.09	8.46 (8.29−8.53)	0.51 (0.33−0.64)
149911	81440	126±16	0.06±0.29	3.970±0.014	1.93±0.12	2.67±0.15	8.61 (8.57−8.65)	0.85 (0.76−0.92)
151525	82216	141±17	−0.64±0.27	3.971±0.014	2.21±0.11	3.04±0.13	8.51 (8.46−8.55)	0.97 (0.92−1.00)
151965	82554	180±28	−0.09±0.35	4.154±0.012	2.38±0.14	3.85±0.19	7.68 (6.25−7.94)	0.26 (0.00−0.50)
152107	82321	53±1	1.21±0.07	3.941±0.015	1.43±0.03	2.10±0.04	8.74 (8.65−8.82)	0.58 (0.48−0.67)
153882	83308	168±20	−0.07±0.27	3.988±0.013	2.00±0.11	2.79±0.14	8.55 (8.51−8.59)	0.84 (0.76−0.91)
154708	84017	140±22	2.90±0.35	3.829±0.013	0.73±0.14	1.43±0.08	9.29 (9.06−9.38)	0.61 (0.33−0.76)
157751	85372	164±28	1.52±0.38	3.993±0.013	1.38±0.15	2.18±0.10	7.56 (7.00−8.45)	0.03 (0.00−0.35)
164258	88148	121±13	0.63±0.24	3.952±0.015	1.67±0.10	2.35±0.11	8.71 (8.66−8.75)	0.75 (0.64−0.83)
165474	88627	130±20	1.75±0.35	3.885±0.011	1.19±0.14	1.82±0.11	8.99 (8.92−9.03)	0.66 (0.51−0.77)
168733	90074	189±27	−1.14±0.31	4.108±0.014	2.70±0.13	4.13±0.25	8.12 (8.08−8.16)	0.87 (0.78−0.94)
168856	90030	179±29	0.28±0.37	4.106±0.014	2.13±0.15	3.28±0.17	7.89 (6.34−8.14)	0.28 (0.00−0.54)
170000	89908	88±3	−0.39±0.10	4.058±0.015	2.28±0.05	3.30±0.08	8.32 (8.27−8.36)	0.78 (0.70−0.84)
170397	90651	87±6	1.14±0.16	4.033±0.016	1.61±0.07	2.48±0.08	7.70 (6.79−8.24)	0.07 (0.00−0.29)
171184	91001	186±35	0.44±0.41	4.081±0.014	2.00±0.17	3.03±0.18	8.02 (6.48−8.25)	0.30 (0.00−0.56)
171586	91142	102±9	1.15±0.21	3.967±0.014	1.48±0.09	2.19±0.08	8.60 (8.43−8.69)	0.48 (0.30−0.61)
172690	93481	249±42	0.19±0.37	4.058±0.015	2.05±0.15	3.00±0.18	8.30 (8.08−8.38)	0.56 (0.32−0.72)
173650	92036	214±34	−0.42±0.35	4.015±0.013	2.20±0.14	3.10±0.20	8.44 (8.39−8.49)	0.86 (0.78−0.93)
175132	92599	374±72	−1.72±0.43	4.022±0.017	2.73±0.17	3.73±0.18	8.27 (8.23−8.32)	1.00 (1.00−1.00)
175362	92989	130±15	−0.40±0.27	4.217±0.013	2.64±0.11	4.64±0.20	6.92 (6.04−7.56)	0.06 (0.00−0.32)
176196	93863	255±44	0.47±0.38	4.000±0.013	1.81±0.15	2.58±0.17	8.53 (8.43−8.59)	0.64 (0.46−0.77)
176232	93179	74±3	1.42±0.11	3.899±0.011	1.32±0.04	1.95±0.04	8.93 (8.88−8.96)	0.71 (0.64−0.77)
179527	94311	300±49	−1.64±0.36	4.046±0.016	2.75±0.15	3.94±0.18	8.22 (8.18−8.26)	1.00 (0.96−1.00)
183056	95556	200±20	−1.28±0.22	4.086±0.014	2.70±0.10	4.08±0.18	8.16 (8.12−8.19)	0.93 (0.87−0.97)
183339	95520	384±76	−1.35±0.43	4.126±0.013	2.82±0.18	4.44±0.37	8.05 (7.99−8.10)	0.88 (0.78−0.96)
183806	96178	133±15	−0.09±0.25	3.983±0.014	2.00±0.10	2.79±0.14	8.56 (8.52−8.60)	0.85 (0.78−0.92)
184905	96292	165±13	0.34±0.18	4.035±0.016	1.93±0.08	2.80±0.09	8.39 (8.26−8.47)	0.57 (0.41−0.69)
187474	97749	103±9	0.32±0.20	4.004±0.013	1.88±0.08	2.67±0.09	8.52 (8.47−8.57)	0.69 (0.58−0.77)
188041	97871	84±6	0.86±0.17	3.926±0.010	1.55±0.07	2.20±0.07	8.80 (8.77−8.83)	0.77 (0.70−0.82)
192678	99672	230±27	0.41±0.26	3.987±0.013	1.81±0.10	2.56±0.12	8.59 (8.54−8.63)	0.71 (0.59−0.80)
196178	101475	147±14	−0.16±0.22	4.126±0.013	2.35±0.09	3.64±0.13	7.99 (7.76−8.09)	0.47 (0.27−0.61)
196502	101260	127±8	−0.36±0.15	3.964±0.014	2.08±0.07	2.87±0.09	8.57 (8.54−8.60)	0.94 (0.90−1.00)
199728	103616	131±17	0.60±0.30	4.078±0.015	1.93±0.12	2.95±0.13	7.89 (6.51−8.21)	0.21 (0.00−0.45)
200177	103658	139±11	1.47±0.18	3.997±0.013	1.41±0.08	2.21±0.07	7.70 (6.99−8.34)	0.05 (0.00−0.27)

Table 2. Continued.

HD	HIP	d (pc)	M_V	log $T_{\rm eff}$ (K)	log $L/L_\odot$	$M/M_\odot$	log t (yr)	τ
201018	104337	174±32	2.32±0.40	3.941±0.015	0.98±0.16	1.82±0.07	7.05 (7.05−8.41)	0.00 (0.00−0.17)
201601	104521	35±1	1.98±0.07	3.882±0.011	1.10±0.03	1.74±0.03	8.99 (8.93−9.05)	0.59 (0.52−0.66)
203006	105382	57±2	1.13±0.11	3.989±0.013	1.52±0.05	2.28±0.05	8.44 (8.23−8.56)	0.37 (0.22−0.49)
204411	105898	119±7	−0.10±0.14	3.942±0.015	1.95±0.06	2.68±0.07	8.65 (8.62−8.68)	0.94 (0.89−0.98)
205087	106355	186±23	0.20±0.28	4.038±0.016	2.00±0.12	2.88±0.14	8.39 (8.28−8.46)	0.63 (0.45−0.75)
208217	108340	146±19	1.50±0.29	3.904±0.011	1.29±0.12	1.93±0.10	8.91 (8.85−8.95)	0.66 (0.52−0.76)
212385	110624	112±11	1.58±0.23	3.923±0.010	1.26±0.09	1.93±0.07	8.80 (8.69−8.86)	0.51 (0.37−0.63)
215038	111849	265±42	0.57±0.35	4.136±0.013	2.08±0.14	3.39±0.14	6.29 (6.26−7.60)	0.00 (0.00−0.16)
216018	112705	109±11	2.51±0.24	3.889±0.011	0.88±0.10	1.63±0.04	8.54 (7.29−8.90)	0.16 (0.00−0.40)
217522	113711	95±8	2.62±0.20	3.816±0.013	0.85±0.08	1.49±0.06	9.33 (9.27−9.40)	0.80 (0.69−0.87)
217833	113797	221±40	−0.52±0.40	4.171±0.012	2.59±0.16	4.23±0.24	7.82 (7.41−7.94)	0.45 (0.16−0.66)
220825	115738	49±1	1.45±0.09	3.958±0.014	1.35±0.04	2.07±0.04	8.57 (8.36−8.70)	0.37 (0.23−0.48)
221006	115908	116±7	0.29±0.14	4.135±0.013	2.19±0.06	3.49±0.10	7.32 (6.26−7.80)	0.08 (0.00−0.27)
221394	116119	147±14	0.45±0.22	3.979±0.014	1.78±0.09	2.51±0.10	8.62 (8.56−8.66)	0.72 (0.61−0.80)
221568	116210	243±39	0.24±0.36	3.962±0.014	1.84±0.14	2.56±0.17	8.65 (8.60−8.70)	0.82 (0.72−0.91)
223640	117629	98±10	0.17±0.22	4.089±0.014	2.13±0.10	3.20±0.12	8.11 (7.84−8.23)	0.44 (0.23−0.60)
224801	63	207±30	−0.43±0.32	4.073±0.015	2.33±0.13	3.41±0.20	8.27 (8.21−8.31)	0.76 (0.62−0.85)